Thematic set:
Carbon forms: paths and processes in the Earth

JGS
Journal of the Geological Society

Published Online First

https://doi.org/10.1144/jgs2018-095

Carbon, carbides, carbonates and carbonatitic melts in the Earth's interior

Vincenzo Stagno

Department of Earth Sciences, Sapienza University of Rome, Rome, Italy
V.S., 0000-0002-8710-0885
Correspondence: vincenzo.stagno@uniroma1.it

Abstract: Over recent decades, many experimental studies have focused on the effect of CO_2 on phase equilibria and melting behaviour of synthetic eclogites and peridotites as a function of pressure and temperature. These studies have been of fundamental importance to understanding the origin of carbonated magmas varying in composition from carbonatitic to kimberlitic. The occurrence of diamonds in natural rocks is further evidence of the presence of (reduced) carbon in the Earth's interior. The oxygenation of the Earth's interior (i.e. its redox state) through time has strongly influenced the speciation of carbon from the mantle to mantle-derived magmas and, in turn, to the volcanic gases released to the atmosphere. This paper explains how the knowledge of the oxygen fugacity recorded by mantle rocks and determined through the use of appropriate oxy-thermobarometers allows modelling of the speciation of carbon in the mantle, its mobilization in the asthenospheric mantle by redox partial melting, and its sequestration and storage during subduction by redox freezing processes. The effect of a gradual increase of the mantle fO_2 on the mobilization of C is here discussed along with the main variables affecting its transport by subduction into the mantle.

Received 9 May 2018; **revised** 6 December 2018; **accepted** 21 December 2018

Carbon in the Earth's mantle is in exchange with the Earth's surface and the atmosphere (Kasting *et al.* 1993). At subduction zones carbon from sediments and altered oceanic crust is transported into the mantle and recycled to the surface on a short timescale as a result of island arc processes, but some carbon probably persists both as carbonate minerals and as elemental carbon during subduction and can be carried down to the depth of the deep upper and even lower mantle (Kelemen & Manning 2015). In contrast, basaltic magmas at mid-ocean ridges and oceanic islands bring carbon mainly in the form of CO_2 to the surface. Some of this carbon shows geochemical evidence of crustal recycling (Hauri *et al.* 1993) but some might result from oxidation of a reduced primordial source; that is, a source present in the mantle since accretion of the Earth (Palot *et al.* 2012). Our understanding of the deep carbon cycle through the mantle requires information on the mobility, solubility within mantle rocks and magmas, and knowledge of the forms in which carbon is stable at different pressure, temperature and oxygen fugacity conditions within the Earth. This information is necessary to determine how much carbon is probably stored in the mantle, and the mechanisms by which it may be cycled through the mantle and eventually reach the surface. In this paper, known forms of carbon-bearing phases found in mantle rocks are first described through a selection of classic articles from the literature, followed by discussion of the carbon speciation as a function of the mantle redox state through space and time.

Current estimates of carbon in the Earth's interior

Estimates of the abundance of carbon in the Earth's interior are uncertain owing to its low solubility in mantle minerals and the outgassing at shallow depths. The amount of carbon in rock-forming minerals such as olivine, orthopyroxene, clinopyroxene and garnet has been determined experimentally and found to be in the range of a few ppm (Keppler *et al.* 2003; Rosenthal *et al.* 2015). Similarly, the most abundant minerals representative of the transition zone and lower mantle (i.e. wadsleyite, ringwoodite, ferropericlase and bridgmanite) also incorporate negligible (<1 ppm) amounts of carbon (Shcheka *et al.* 2006; Hayden & Watson 2008). The low concentration of carbon in the abundant silicate minerals implies that it must be stored in the largest geochemical reservoir, the terrestrial mantle (Javoy *et al.* 1982), as a pure phase in the immobile reduced form of elemental carbon (or carbide), oxidized carbonate and the mobile form of carbonated magma. Because of the low solubility of CO_2 in magmas upon decompression with consequent devolatilization, the possibility of tracking its history from the source rock to the surface is limited to a few known undegassed lavas (e.g. Siqueiros and 2πD43 popping rocks; Le Voyer *et al.* 2017); alternatively, geochemical tracers and noble gases that correlate positively with the abundance of C (e.g. helium, argon, barium, rubidium and niobium; Matthews *et al.* 2017) are used, the concentrations of which are better constrained because of their high incompatibility in erupted lavas and sampled fumaroles. Using, then, the global average concentration of these trace elements from mid-ocean ridge basalts (MORB) and assuming typical melt fractions of 10%, such a method provides concentrations of a few tens of ppm (*c.* 14–50 ppm) as referred to the depleted mantle (i.e. the residual mantle source after extraction of MORB); whereas the carbon content of the bulk silicate Earth (BSE), generally determined from mantle plume-like magmas, has been proposed to vary between 500 and 1000 ppm (Marty *et al.* 2013).

Different forms of elemental carbon in mantle rocks: graphite, diamonds and carbides

Carbon forms different accessory phases in rocks from the Earth's interior, such as graphite, diamond, iron(–nickel) and silicon carbides and either solid or liquid carbonates. Native carbon in mantle-derived rocks such as eclogites and peridotites occurs both as graphite and diamond. The origin of graphite in mantle-derived rocks is usually explained as a result of the following: (1) transformation from an original diamond-bearing assemblage to graphite owing to a re-emplacement at lower pressures observed, for

example, in garnet pyroxenite layers from Beni Bousera, Morocco (Pearson *et al.* 1989); (2) exsolution from a C-saturated magma at reducing conditions as observed in ultramafic xenoliths from the Algerian Sahara (Kornprobst *et al.* 1987); or (3) as a relict of metasomatic processes such as found in peridotites from Jagersfontein (South Africa) showing multiple graphite flakes of vein-like form (Field & Haggerty 1990). Some graphite occurrences are thought to originate by assimilation from magma of carbonaceous country rocks (Ripley & Taib 1989; Barrenechea *et al.* 1997; Luque *et al.* 1998). In contrast to the processes above, where variation in pressure, temperature and bulk-rock chemistry are invoked to explain the origin of graphite, there is also evidence of crystalline carbon in exhumed blueschist metasedimentary rocks in contact with serpentinite from Alpine Corsica (France) that formed by reduction of carbonate during cold subduction (Galvez *et al.* 2013).

In contrast to what observed for graphite, the occurrence of diamonds is limited to specific rock types, mainly kimberlites but also lamproites and lamprophyres from cratonic areas (Boyd & Gurney 1986; Gurney *et al.* 2010), regions of the continental crust that have remained tectonically stable for at least 2.5 Gyr and are underlain by a thick lithospheric mantle extending to depths of over 200 km. Rocks considered as host for diamonds have been identified on the basis of inclusions in natural diamonds and are represented by eclogites (E-type inclusions), peridotites and websterites (P-type inclusions; Meyer 1987; Gurney 1989; Stachel & Harris 2008). The occurrence of carbon in the form of diamond has been a major field of research because of its economic value and stimulated some of the very first high-pressure experiments (Bundy 1963; Kennedy & Kennedy 1976; Akaishi *et al.* 1990; Irifune *et al.* 2004) that aimed to explore the pressure and temperature conditions for synthesis of gem-like quality diamonds. The results from these studies combined with thermodynamic predictions (Day 2012) have been used as a geothermobarometer to constrain the equilibration pressures and temperatures of diamond-bearing rocks, in particular those rocks showing coexistence between graphite and diamond (e.g. Korsakov *et al.* 2010; Mikhailenko *et al.* 2016). Importantly, most attention has been paid to the chemical composition of minerals and fluids trapped in diamonds as a tool to understand their origin. For instance, this is the case for silicate minerals from Juina diamonds (Walter *et al.* 2008) and daughter minerals in fibrous diamonds (Weiss *et al.* 2011), both showing geochemical evidence of the passage of CO_2-rich melts with important implications for the origin of diamonds by reduction of C–O(–H) mantle fluids.

Although rarely found in nature, carbon can be stored also as silicon carbide (Leung *et al.* 1990; Mathez *et al.* 1995; Yang *et al.* 2015) or as an alloying element in Fe(–Ni) metal trapped in diamonds (Jacob 2004; Kaminsky & Wirth 2011; Mikhail *et al.* 2014; Smith *et al.* 2016). The stability of Fe(–Ni)–C intermetallic alloys has been the subject of investigation in recent high-pressure experimental studies (Fei & Brosh 2014; Rohrbach *et al.* 2014; Stagno *et al.* 2014) and, in the mantle, this appears strongly dependent on the ratio between metallic iron and elemental carbon and, therefore, mostly associated with local heterogeneities in the C/Fe distribution. In fact, assuming that the deep mantle at depth below *c.* 300 km is saturated with 1 wt% Fe(Ni) alloy (Frost *et al.* 2004; Rohrbach *et al.* 2011), most of the elemental carbon is predicted to dissolve with concentrations up to 2 wt% in the alloy. This implies that, where elemental carbon is locally more abundant (>*c.* 100 ppm) than iron, carbides can be stable in the form of molten Fe_7C_3 along with coexisting diamonds (Dasgupta & Hirschmann 2010; Rohrbach *et al.* 2014). Therefore, carbides would form by solid–solid reaction only in portions of the Earth's interior where iron metal and elemental carbon (either graphite of diamonds) or carbonate (Palyanov *et al.* 2013) are in mutual contact. Thus, one should not be surprised if the best evidence of Fe-carbides in the mantle is probably produced by solid–solid reaction at the boundary between the Fe inclusions and the diamond host at mantle conditions (Kaminsky & Wirth 2011; Smith *et al.* 2016). The local mantle oxidation state also plays a critical role in determining the conditions for the stability of carbide versus carbonate phases.

Carbonate minerals and CO_2-bearing melts

Carbon occurs in the mantle in its oxidized form (e.g. C^{4+}); for example, as either solid or molten carbonate or fluid where it can be present as both molecular (CO_2) and ionic (CO_3^{2-}) species. Carbonate minerals are usually solid solutions between calcite ($CaCO_3$), magnesite ($MgCO_3$) and siderite ($FeCO_3$) end-members strongly depending on the temperature, pressure and bulk composition (see Hammouda & Keshav 2015, and references therein). A Ca, Mg-rich phase (dolomite) is stable below 4 GPa (*c.* 120 km) in peridotite assemblages (Falloon & Green 1989, 1990), whereas Ca-rich solid carbonates are shown experimentally to be stable in eclogitic assemblages (Hammouda 2003; Yaxley & Brey 2004). As the pressure increases, magnesite is expected to be the stable carbonate with respect to dolomite and siderite as a consequence of the high affinity of Ca and Fe for lower mantle silicate minerals (see Fig. 1a; Hammouda 2003; Ghosh *et al.* 2009; Litasov & Ohtani 2009*a*,*b*, 2010; Keshav & Gudfinnsson 2010; Stagno *et al.* 2011; Kiseeva *et al.* 2013). However, previous experimental studies support the observation of Mg-rich carbonates

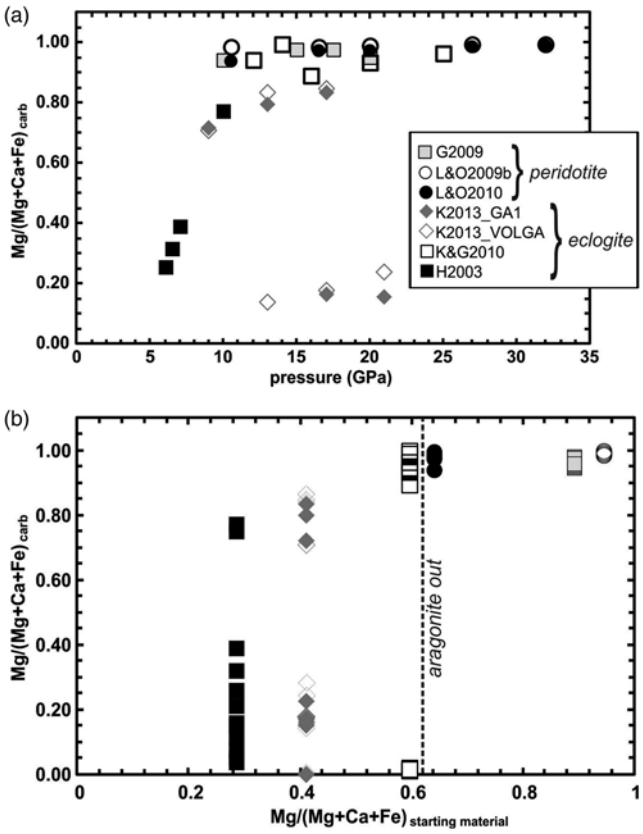

Fig. 1. Chemical composition of solid carbonates recovered from multi-anvil experiments at pressures up to 32 GPa expressed as Mg/(Mg + Ca + Fe) molar ratio v. pressure (**a**) and v. Mg/(Mg + Ca + Fe) of the employed starting material from (sub)solidus synthetic peridotite and eclogite mineral assemblages (**b**). Data sources: G2009, Ghosh *et al.* (2009); L&O2009b, Litasov & Ohtani (2009*b*); L&O2010, Litasov & Ohtani (2010); K&G2010, Keshav & Gudfinnsson (2010); K2013, Kiseeva *et al.* (2013); H2003, Hammouda (2003).

and aragonite coexisting for Mg# of the initial starting material of ≤0.6 (Fig. 1b). The presence and chemical composition of solid carbonates coexisting with mantle minerals are determining factors for the composition of near-solidus CO_2-rich magmas formed by partial melting of carbonated eclogites and peridotites (Gudfinnsson & Presnall 2005; Hammouda & Keshav 2015, and references therein). Carbonatites are defined by the Subcommission on the Systematics of Igneous Rocks of the International Union of Geological Sciences (IUGS) as igneous rocks, either effusive or intrusive, containing more than 50% in volume of primary carbonate minerals (Streckeisen 1980); that is, the result of crystallization of a magma with less than 10 wt% of SiO_2 (Woolley & Kempe 1989). Carbonatites have been found in several localities within diverse geological settings related to either intraplate continental rifts or compressive systems such as subduction zones (for more details on the worldwide distribution, see Woolley & Kjarsgaard 2008), although a mantle origin for these liquids is not unequivocal (Koster van Groos & Wyllie 1963; Wyllie & Huang 1975; Wallace & Green 1988; Veksler *et al.* 1998) as they might retain evidence of crustal origin (Liu *et al.* 2016) and late-stage assimilation processes (Lustrino *et al.* 2016). Primary carbonatitic melts were shown experimentally to be characterized by extremely low viscosity in the range of 0.003 and 0.01 Pa s (Kono *et al.* 2014; Stagno *et al.* 2018), other than being an important constituent of metasomatic fluids interacting with mantle silicates in peridotite xenoliths from Spitsbergen in Norway (Ionov *et al.* 1993); and their possible origin beneath mid-ocean ridges has been the subject of several experimental studies (Dasgupta & Hirschmann 2006 ; Stagno *et al.* 2013) aimed at shedding light on the seismic and electrical conductivity anomalies in the upper mantle as detected beneath the East Pacific Rise ocean ridge (Evans *et al.* 1999; Dunn *et al.* 2001; Gu *et al.* 2005; Gaillard *et al.* 2008).

Kimberlitic magmas are thought to form at depths below 150 km by partial melting of a carbonated mantle rock source and are also important carriers of carbon either in the form of a dissolved CO_3^{2-} component in the melt, or as exsolved CO_2 or diamonds. Diamonds found in kimberlites, such as those from Lac de Gras (Canada), are known for showing morphological features typical of surface dissolution that link with the oxidizing nature of these melts (Gurney *et al.* 2004; Fedortchouk *et al.* 2005) during their ascent at conditions where diamonds become unstable. The local oxygen fugacity has, therefore, the potential to flux carbon out the Earth's interior, with implications for its residence time.

The speciation of carbon as a function of pressure, temperature and Earth's mantle redox state

To date, many experimental studies have been performed to investigate the structural stability of pure carbonate minerals (Biellmann *et al.* 1993; Isshiki *et al.* 2004; Oganov *et al.* 2008; Mao *et al.* 2011; Boulard *et al.* 2012; Cerantola *et al.* 2017) and their melting (Tao *et al.* 2013; Solopova *et al.* 2014; Shatskiy *et al.* 2015*a*,*b*) as well as melting of CO_2-bearing mineral mantle assemblages as a function of pressure and temperature, respectively (for a detailed reference list see Hammouda & Keshav 2015). All these experimental studies, however, assume the stability of carbonate minerals at depth, neglecting the possibility that elemental carbon rather than carbonate can be the stable carbon phase depending on the availability of oxygen in the interior of the Earth. An alternative and more dynamic approach to understanding the state of carbon at depth is to consider the oxygen fugacity required for carbonate (liquid or solid) to be stable versus elemental carbon. The fO_2 in the Earth's interior is buffered by the local abundant silicate minerals and is dependent on the pressure and temperature. Only when the fO_2 required for the carbon–carbonate equilibrium crosses the local fO_2 buffered by the mantle rocks will oxidation of diamonds to solid carbonates occur and, at solidus T, CO_2-rich magmas can form. In the next section, we will review some recent studies on the calibration of oxy-thermobarometers that are widely used to determine the oxidation state of mantle peridotites and eclogites and, thus, model the speciation of carbon throughout the Earth's interior. In addition, some redox reactions of interest for the speciation of carbon down to the lower mantle will be discussed.

The oxygen fugacity and its application in experimental petrology

The oxygen fugacity (fO_2), or partial pressure of oxygen (Eugster 1957), is the thermodynamic variable that indicates the chemical potential (i.e. availability) of oxygen in those reactions where both reagents and products contain the same element(s) but with different oxidation states. These reactions are termed redox reactions and their graphical representations are univariant curves in log fO_2–temperature diagrams. At a given temperature, above this curve the oxidized phase of an assemblage is stable, whereas below it the reduced phase is stable (see Fig. 2). Rock-forming minerals are widely characterized by the presence of heterovalent elements, such as iron, chromium and vanadium. Their occurrence in oxidized or reduced form can be used to infer the redox state at which certain rocks have equilibrated. An important goal in experimental geochemistry is, therefore, to investigate the behaviour of these elements with respect to the fO_2 and develop interpretative models to understand the change of redox conditions in the Earth and how this might have influenced the speciation of carbon (Delano 2001; Li & Lee 2004; Aulbach & Stagno 2016).

The fO_2 in experiments performed at high pressure and temperature is monitored mainly following two techniques: the first is based on the use of solid minerals or metal–metal oxide couples (e.g. Fe–FeO, Re–ReO_2, Mo–MoO, Ni–NiO, etc.) that buffer the oxygen fugacity at certain known values calculated using the relative thermodynamic data and equation of states; the second approach employs noble metals as redox sensors to effectively measure the unknown oxygen fugacity of the run products

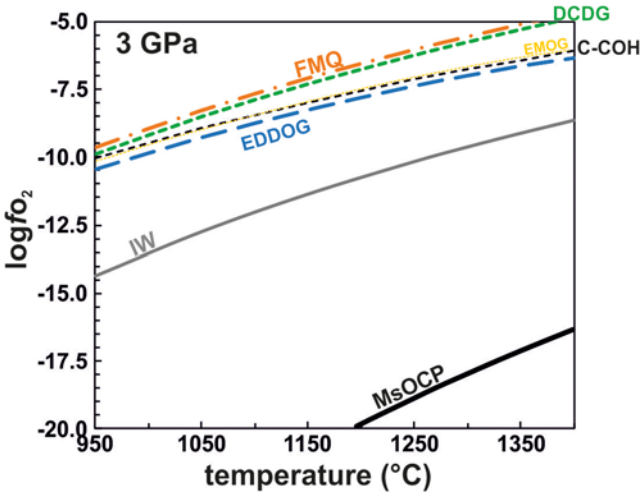

Fig. 2. Logarithm of the oxygen fugacity (log fO_2) v. temperature (°C) diagram of redox buffers commonly employed in petrology of C phases. Calculations are performed at 3 GPa and temperatures between 950 and 1400°C. Buffer abbreviations: FMQ, fayalite–magnetite–quartz buffer (O'Neill 1987); DCDG, dolomite–coesite–diopside–graphite buffer (Luth 1993); EMOG, enstatite–magnesite–olivine–graphite, and EDDOG, enstatite–dolomite–diopside–olivine–graphite buffers (Stagno & Frost 2010); IW, iron–wüstite buffer (O'Neill 1987); C–COH, graphite–COH fluid (Ulmer & Luth 1991); MsOCP, moissanite–olivine–graphite–enstatite (Ulmer *et al.* 1997).

recovered from a given pressure and temperature. In more detail, these techniques can be summarized as follows.

(1) Double capsules are used, where an outer capsule (e.g. of Re) contains a metal oxide (e.g. ReO_2) buffer and H_2O and an inner capsule contains the sample plus H_2O. A Pt inner capsule ensures permeability of H_2 between the buffering outer and the inner capsules. By buffering the fH_2 in the outer capsule the fO_2 of the inner capsule is fixed (Eugster & Wones 1962; Ulmer & Luth 1991).

(2) Capsules of materials such as Fe, Re and BN have been shown to influence the redox state of samples (Wendlandt *et al.* 1982; McCammon & Ross 2003), although a fluxing phase (i.e. a circulating fluid) is necessary to ensure homogeneous fO_2 conditions inside the whole capsule.

(3) Buffering solid assemblages such as a mixture of Re and ReO_2 can be added (about 15–20 wt%) to the starting material (Rubie 1999). In this case, the fO_2 of the experiment is buffered by the solid assemblage only if both metal and metal oxide phases coexist and are in mutual contact with the surrounding mineral assemblage. The circulation of a fluid phase would also help to buffer the fO_2 all over the sample. Obviously, the choice of the metal–metal oxide depends on its potential reactivity with the experimental starting materials, which would limit its applicability.

(4) Noble metal alloys (e.g. platinum group elements (PGE), Au and Ag) are used as sliding redox sensors where the fO_2 is measured (not buffered), which normally comprise an Fe-bearing metal alloy (Huebner 1971; Taylor *et al.* 1992).

The first three experimental techniques allow investigation of the dependence of a variable (e.g. $Fe^{3+}/\Sigma Fe$ in minerals, element partitioning, C–O–H fluid speciation, melting temperature) with respect to the buffered (imposed) known fO_2. In contrast, the application of noble metals (mainly platinum and iridium) employed as redox sensor is more appropriate when the fO_2 buffered by a mineral assemblage is quantitatively not known, meaning that its variation as a function of P–T needs to be determined (i.e. the univariant curve in the log fO_2 versus T or P diagram), or when the fO_2 buffered by a solid mineral assemblage (although it can be calculated using a proper thermodynamic dataset of the mineral end-members (Luth 1993) involved) needs to be verified owing to its use at extrapolated P–T conditions or owing to the disappearance of a phase (e.g. by melting). A practical example is given by the coexistence of graphite (diamond) and carbonate along with mantle silicates in peridotite (known by the acronym EDDOG/D) and eclogite (DCDG/D) mineral assemblages as follows:

$$\underset{\text{enstatite}}{2Mg_2Si_2O_6} + \underset{\text{dolomite}}{CaMg(CO_3)_2} = \underset{\text{diopside}}{CaMgSi_2O_6} + \underset{\text{olivine}}{2Mg_2SiO_4} + \underset{\text{graph/diam}}{2C} + 2O_2 \quad (1)$$

and

$$\underset{\text{dolomite}}{CaMg(CO_3)_2} + 2SiO_2 = \underset{\text{diopside}}{CaMgSi_2O_6} + \underset{\text{graph/diam}}{2C} + 2O_2. \quad (2)$$

Equilibria (1) and (2) are both chosen to represent the fO_2 at which carbon is present either as graphite (or diamond, C^0) or carbonate (C^{4+}) along with mantle mineral assemblages. The fO_2 buffered by both equilibria was calibrated based on a set of thermodynamic data for each pure phase by Eggler & Baker (1982) and Luth (1993), respectively (Fig. 2). However, the fO_2 buffered by equilibria involving solid carbonates is applicable only at temperatures below their melting temperature. Above the melting (solidus) temperature, the fO_2 will be buffered by similar equilibria to (1) and (2) where the solid carbonate is replaced by the CO_2-rich silicate-bearing melt. Because thermodynamic data are complex to determine and not available for liquid carbonates, the composition of which varies as the temperature increases toward more and more SiO_2-rich liquids, accurate measurements of the fO_2 at each P and T are necessary. These can be made by adding 3–5 wt% of pure Ir (or Pt) metal as a redox sensor to the starting material. During the high P–T experiment, FeO from the coexisting phases (i.e. equilibria (3) and (4)) is reduced to Fe^0 and alloys with the Ir metal. The activity of Fe in the alloy is adjusted to the value buffered by the presence of carbonate melt and graphite (or diamond; equilibria (1) and (2)) at a given P and T. The resulting lowering of the activity of the Ir (Pt) metal component is a consequence of the redox conditions imposed by the carbon–carbonate equilibrium as a function of pressure and temperature and the melt composition. The fO_2 at which carbon and carbonate coexist within synthetic peridotite and eclogite assemblages (1) and (2) at high P–T of the experiments is, thus, calculated using the simultaneous mineral equilibria

$$\underset{\text{olivine}}{Fe_2SiO_4} = SiO_2 + \underset{\text{alloy}}{2Fe} + O_2 \quad (3)$$

and

$$\underset{\text{garnet}}{Fe_3Al_2Si_3O_{12}} = \underset{\text{kyanite}}{Al_2SiO_5} + \underset{\text{coesite}}{2SiO_2} + \underset{\text{alloy}}{3Fe} + 1.5O_2. \quad (4)$$

The fO_2 of the above equilibria is then calculated with the formulae

$$\log fO_2 = \frac{-\Delta rG^{\circ}_{P,T}[3]}{RT\ln(10)} + \log a^{\text{olivine}}_{Fe_2SiO_4} - \log a_{SiO_2} - 2\log a^{\text{alloy}}_{Fe} \quad (5)$$

and

$$\log fO_2 = \frac{-\Delta rG^{\circ}_{P,T}[4]}{1.5RT\ln(10)} - 2\log a^{\text{alloy}}_{Fe} + \frac{2}{3}\log a^{\text{garnet}}_{Fe_3Al_2Si_3O_{12}}. \quad (6)$$

A gradual decrease of the measured fO_2 buffered by equilibria (1) and (2) is observed as result of the increased SiO_2 content of the carbonated melt with temperature in contrast to thermodynamic calculations of the fO_2 buffered by the appropriate subsolidus peridotitic and eclogitic assemblage (Stagno & Frost 2010; Stagno *et al.* 2015).

The choice of including kyanite in equilibrium (4) is mainly motivated by the need to balance the excess of Al from the involved almandine component, although also supported by its presence in diamantiferous eclogites (Smyth 1980; Mikhailenko *et al.* 2016). Because Al_2SiO_5 and SiO_2 are pure phases in natural eclogites (e.g. Mikhailenko *et al.* 2016), the fO_2 in (6) is calculated fixing the activity of these phases at unity, and $a^{\text{olivine}}_{Fe_2SiO_4}$, a^{alloy}_{Fe}, a_{SiO_2} and $a^{\text{garnet}}_{Fe_3Al_2Si_3O_{12}}$ are the activities of the Fe_2SiO_4 component in olivine, Fe in Fe–Ir alloy and the $Fe_3Al_2Si_3O_{12}$ component of garnet, respectively, calculated using the appropriate activity–composition models (Stagno & Frost 2010; Stagno *et al.* 2015). $\Delta rG_{P,T}$ is the standard state Gibbs free energy change of pure end-member equilibria (3) and (4), determined at the pressure and temperature of interest from the thermodynamic data (i.e. formation enthalpy, entropy, heat capacity, thermal expansivity, molar volume) and the equation of state of each mineral end-member (details have been given by Stagno & Frost 2010; Stagno *et al.* 2015). A full formulation of the $\Delta rG_{P,T}$ has been given by Cemič (2005),

$$\Delta_r G^0_{P,T} = \Delta_r H_{298} + \int_{298}^{T} \Delta_r C_p dT - T\left[\Delta_r S_{298} \int_{298}^{T} (\Delta_r C_p/T)dT\right] + [\Delta_r V_{298} + \Delta_r(\alpha_i V_{i,298})(T - 298) - \frac{\Delta_r(\beta i V_{i,298})P}{2}(P - P_0) = 0 \quad (7)$$

where $\Delta_r H_{298}$, $\Delta_r S_{298}$, $\Delta_r C_p$ and $\Delta_r \alpha$ are the enthalpy and entropy of formation, heat capacity and thermal expansivity changes of the

reaction (Fei 1995; Fabrchanaya *et al.* 2004); $\Delta_r V$ is the volume change of a reaction, i is the ambient pressure and temperature volumes times their appropriate thermal expansivity and β is the compressibility. a_{Fe}^{metal} is the activity of Fe in the Ir–(Pt–)Fe alloy determined as

$$a_{Fe}^{metal} = X_{Fe}^{metal}\gamma_{Fe}^{metal} \quad (8)$$

where X_{Fe}^{metal} is the molar Fe/[Fe + Ir(or Pt)] in the alloy and γ_{Fe}^{metal} is the activity coefficient of Fe in the alloy determined using symmetric binary Margules terms provided in the literature (Schwerdtfeger & Zwell 1968; Kessel *et al.* 2003). Many noble metals that form solid solutions with Fe can be employed as a redox sensor. Fe–Ir and Fe–Pt are preferred because Fe is likely to exist in the face-centred cube (FCC) structure over the experimental pressure and temperature range of multi-anvil applications. Further, the solubility of C in Ir and Pt has been shown to be negligible at least in the recovered run products (Stagno *et al.* 2011, 2015). Importantly, timescales of the order of 12–24 h are required for the equilibrium fO_2 to be obtained. Although an important aspect in facilitating equilibrium is to keep the grain size of the initial Ir and Pt metals at *c.* 5 μm to accelerate the diffusion of Fe from the surrounding silicate minerals, the equilibration becomes sluggish at subsolidus temperatures, with consequent unequilibrated fO_2 (Stagno *et al.* 2015). A further source of uncertainty is represented by the possible overestimation of XFe in the alloy caused by secondary X-ray fluorescence near grain boundaries (Llovet & Galan 2003). For instance, an overestimation of the XFe mole fraction in the alloy by ±0.01 (i.e. ±0.4 wt% Fe) would result in a difference in the calculated fO_2 of about ±0.3 log units. The presence of oxides measured in the alloy, such as SiO_2 and CaO, probably results from the contribution of nearby silicates, and it can be used to evaluate the quality of the electron microprobe measurements on the redox sensor alloy.

The mantle redox state and the speciation of carbon over time

The redox state of the upper mantle refers to the oxygen fugacity of unaltered spinel and garnet peridotites and eclogites equilibrated at depths from 45–60 km (e.g. spinel lherzolites from the Vitim Field; Ionov *et al.* 2005; Goncharov & Ionov 2012) to *c.* 255–270 km (e.g. garnet peridotite from the Diavik Mine, Slave Craton; Creighton *et al.* 2009; kyanite-bearing eclogite from the Lace kimberlite, Kaapvaal Craton; Aulbach & Viljoen 2015) and ranging in age from *c.* 3.8 to *c.* 2.6 Ga. The knowledge of the fO_2 recorded by these rocks is made possible through the use of oxy-thermobarometers; that is, redox equilibria representative of peridotitic and eclogitic mantle mineral assemblages where Fe in the form of Fe^{2+} and Fe^{3+} occurs both as reagents and products as follows:

$$\underset{\text{fayalite}}{6Fe_2^{(2+)}SiO_4} + O_2 = \underset{\text{ferrosilite}}{3Fe_2^{(2+)}Si_2O_6} + \underset{\text{magnetite}}{2Fe^{(2+)}Fe_2^{(3+)}O_4} \quad (9)$$

$$\underset{\text{grossular}}{2Ca_3Al_2Si_3O_{12}} + \underset{\text{fayalite}}{4Fe_2^{(2+)}SiO_4} + \underset{\text{enstatite}}{6MgSiO_3} + O_2$$
$$= \underset{\text{andradite}}{2Ca_3Fe_2^{(3+)}Si_3O_{12}} + \underset{\text{pyrope}}{2Mg_3Al_2Si_3O_{12}} + \underset{\text{ferrosilite}}{4Fe^{(2+)}SiO_3} \quad (10)$$

$$\underset{\text{hedenbergite}}{5CaFe^{(2+)}Si_2O_6} + \underset{\text{grossular}}{\tfrac{1}{3}Ca_3Al_2Si_3O_{12}} + O_2$$
$$= \underset{\text{andradite}}{2Ca_3Fe_2^{(3+)}Si_3O_{12}} + \underset{\text{almandine}}{\tfrac{1}{3}Fe_3^{(2+)}Al_2Si_3O_{12}} + \underset{\text{quartz/coesite}}{4SiO_2}. \quad (11)$$

The Gibbs free energy change of these chemical equilibria was calibrated experimentally at P–T applicable to mantle depths

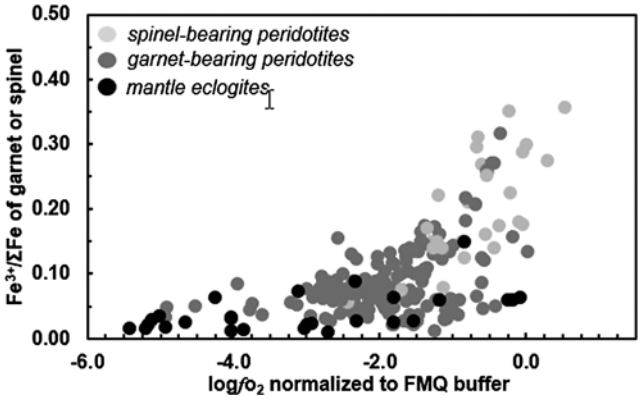

Fig. 3. Ferric iron content of garnet and spinel from mantle rocks plotted as a function of the calculated log fO_2 using equations (9)–(11). Data from garnet- and spinel-bearing peridotites are from Miller *et al.* (2016) and Stagno *et al.* (2013). Data on eclogites are from Stagno *et al.* (2015, and references therein) and Aulbach *et al.* (2017).

employing the redox sensor technique (O'Neill 1987; Ballhaus *et al.* 1991; Gudmundsson & Wood 1995; Stagno *et al.* 2013, 2015). The use of these oxy-thermobarometers requires measurements of the Fe^{3+} content in natural Cr-bearing spinel (equation (9)), and garnet (equations (10) and (11)) in addition to the chemical composition of the coexisting silicates. Figure 3 shows the Fe^{3+} content of Cr-spinel and garnet of natural mantle peridotites and eclogites available in the literature plotted as a function of the calculated fO_2. The positive correlation between $Fe^{3+}/\Sigma Fe$ of spinel or garnet and the log fO_2 is evident and brings into consideration that most of the spinel peridotite xenoliths are more oxidized than garnet peridotite and eclogites. Natural spinels are characterized by averaged $Fe^{3+}/\Sigma Fe$ contents of 22(±8)%, whereas garnets from peridotites and eclogites show much lower averaged contents of *c.* 8 (±5)% and 4(±3)%. Because of the coexistence of many of these xenoliths with graphite and/or diamonds, the correlation between $Fe^{3+}/\Sigma Fe$ and the mantle redox state reflects the chemical potential of these rocks to reduce or oxidize volatile phases such as C through the general net redox reaction

$$4Fe_{(bulk)}^{3+} + C^0 = 4Fe_{(bulk)}^{2+} + C_{vap/melt/solid}^{4+} \quad (12)$$

where Fe^{3+} and Fe^{2+} refer to the ferric and ferrous iron of the bulk-rock. Indeed, a similar equilibrium can be written replacing C^0 and C^{4+} with H_2 and H^+, N^{3-} and N_2, and S^{2-} and S^{6+}, respectively, to describe the buffering effect of Fe-bearing silicates on the speciation of (less abundant) volatiles. The redox state of the lithospheric mantle as a function of equilibrated depth is shown in Figure 4, where most of the peridotitic xenoliths plot in the diamond and graphite stability field possibly along with C–O(–H) fluids or melts from carbonatitic to kimberlitic in composition. The fO_2 required for carbide phases to coexist along with mantle silicates would be 7–8 log units below the FeNi precipitation curve (Fig. 4) as predicted by Schmidt *et al.* (2014). In contrast, most of the fibrous diamonds show inclusions of daughter minerals probably crystallized from a CO_2-rich melt (the growth medium) suggesting, therefore, an fO_2 for their formation near the equilibrium between diamonds and molten carbonate between −1 and −2.5 log units at P–T conditions of the cratonic geotherm (44 mW m^{-2} is here taken as reference). In addition, the oxidation state of most of the eclogitic rocks is shown to plot in the diamond stability field within a range of fO_2 values consistent with those of peridotite xenoliths. A few eclogitic xenoliths from the Lace kimberlites (Aulbach *et al.* 2017) appear reduced (log fO_2 between FMQ −4 and FMQ −5, where FMQ is fayalite–magnetite–quartz buffer) and might have coexisted, therefore, with CH_4-rich fluids. Such overlap might reflect either

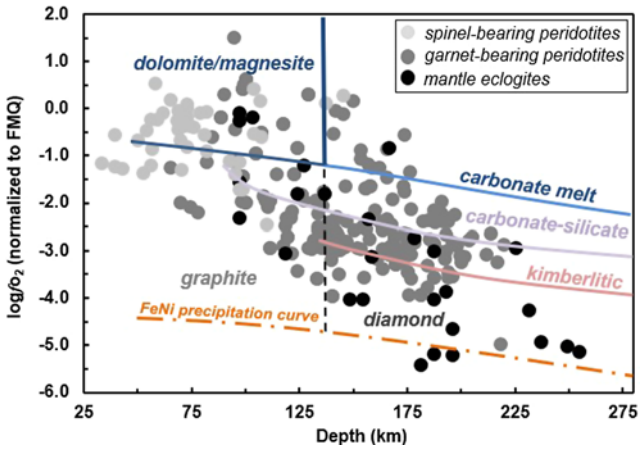

Fig. 4. Log fO_2 (normalized to the FMQ buffer) calculated for mantle xenoliths using oxy-thermobarometers (9), (10) and (11). The blue curve is the oxygen fugacity calculated for equilibrium (1) along a cratonic geotherm of 44 mW m^{-2} that defines the stability field for diamond (or graphite) and solid (liquid) carbonate. The purple and pink curves indicate equilibrium fO_2 between diamonds and a carbonate–silicate and kimberlitic melt, respectively, calculated along a cratonic geotherm. The orange line is the FeNi precipitation curve (Frost & McCammon 2008). References are as in Figure 3.

Fe^{3+} depletion of the protolith or the result of metasomatism. A more detailed explanation is given below.

The redox profile of the subducted slab and the transport of carbon to the deep mantle

The subduction of carbon back into the mantle is an important natural form of carbon sequestration and recycling (Kelemen & Manning 2015). The residence time, storage and flux in or out of carbon in the eclogitic portions of the slab mainly depend on the redox conditions buffered by the surrounding mineral phases represented by equilibrium (11). Carbonate minerals subducted into the deep mantle can undergo important polymorphic transformations such as that from rhombohedral dolomite-I to triclinic dolomite-II at 17 GPa to dolomite-III at *c.* 35 GPa, which makes them an important carrier of C down to the lower mantle (Mao *et al.* 2011). Subducted carbonates are also exposed to melting processes at variable depths depending on the bulk-rock chemistry and *P*–*T* path (Hammouda & Keshav 2015). A recent experimental study by Thomson *et al.* (2016) showed that melting of a carbonated MORB is expected to occur at depth between *c.* 330 and 580 km with the production of Na-bearing carbonatitic melts representing, therefore, a 'barrier' to further subduction of carbonate minerals. Although these melts are important metasomatic agents potentially responsible for the refertilization of the asthenospheric mantle (Rosenthal *et al.* 2014), the interaction with the surrounding Fe metal-saturated mantle can cause their reduction to diamonds by redox freezing (Rohrbach & Schmidt 2011). Inclusions in superdeep diamonds such as majorite and Ca-silicates (Thomson *et al.* 2016) were claimed to form by interaction of alkali-rich carbonatitic melts and reduced asthenospheric mantle. Importantly, the fate of the subducted carbonates at depth is also strongly linked with the intrinsic redox state of the oceanic slab buffered by Fe-bearing phases such as clinopyroxene and garnet. These minerals can significantly become oxidized and, thus, incorporate a large amount of Fe^{3+} as a result of increasing depth (i.e. pressure) at the expense of the surrounding available oxygen (Stagno *et al.* 2015). This form of oxygen sequestration from Fe-bearing minerals can result in reduced portions of the subducted slab with diamond being the stable C form even at an fO_2 higher than that required for diamonds to be stable in peridotites (i.e. $fO_{2[DCDG/D]} > fO_{2[EMOG/D]}$) as in Fig. 2; Luth 1993). A tentative reconstruction of the redox state of the subducted slab as a function of depth is shown in Figure 5a and b.

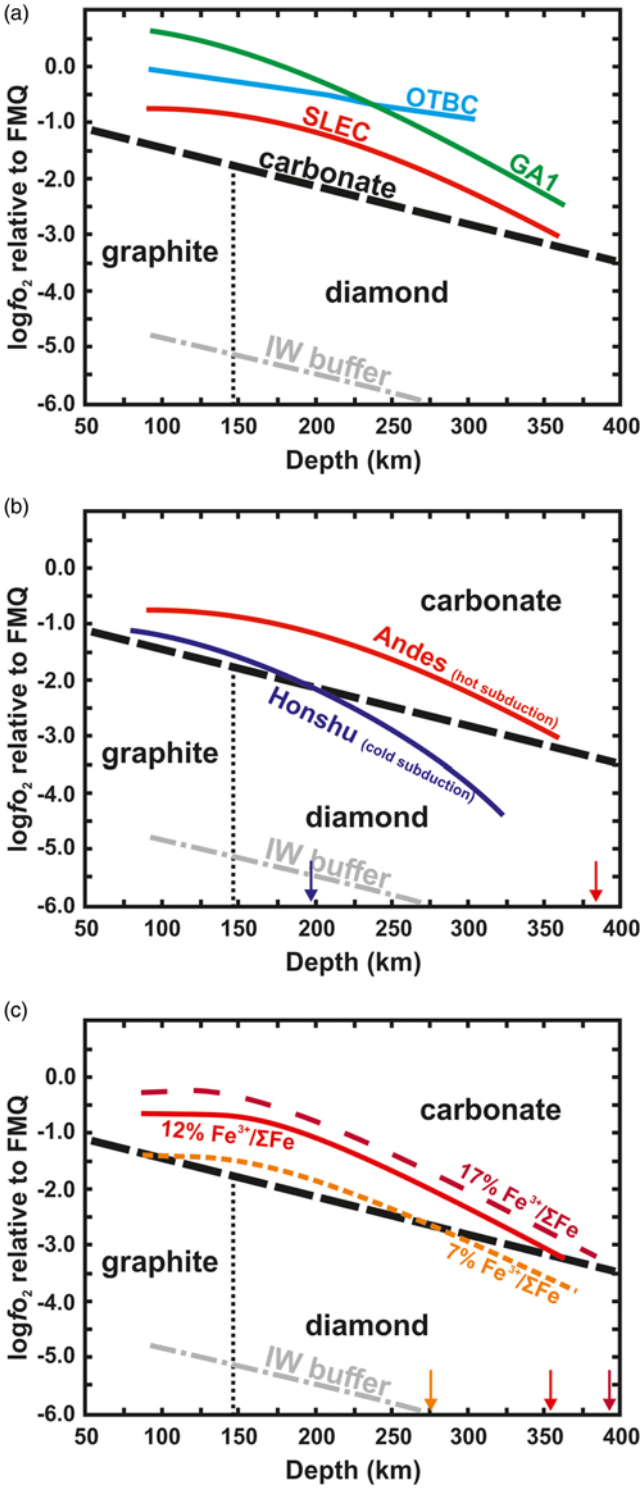

Fig. 5. (**a**) The fO_2 of subducted eclogitic rocks is calculated along a hot subduction geotherm assuming bulk $Fe^{3+}/\Sigma Fe$ ratios of 12% that describes the ratio determined for modern-day MORB glasses (Cottrell & Kelley 2011) and for different bulk chemical compositions for synthetic eclogites in the literature (GA1, Yaxley & Green 1994; SLEC, Dasgupta *et al.* 2005; OTBC, Hammouda 2003). The fO_2 at which carbonate minerals or melts would reduce to graphite or diamond within eclogitic rock is also shown (bold black dashed line; Luth 1993). In (**b**) the fO_2 is determined for an eclogitic assemblage with a MORB bulk composition along a hot and cold subduction geotherm as for the Andes and Honshu respectively (Syracuse *et al.* 2010). In (**c**) the fO_2 is determined for an eclogitic assemblage with a MORB bulk compositions with $Fe^{3+}/\Sigma Fe$ ratio of 0.07, 0.12 and 0.17.

Here, the variation of fO_2 is calculated using the equilibrium (equation (11)) for an eclogitic slab with different bulk composition (Fig. 5a; GA1, Yaxley & Green 1994; SLEC, Dasgupta *et al.* 2005; OTBC, Hammouda 2003), different temperature regime (Fig. 5b; cold and hot subduction, Syracuse *et al.* 2010) and different $Fe^{3+}/\Sigma Fe$ content to reflect the different oxidation state of the MORB protolith (Fig. 5c; Cottrell & Kelley 2011) along with the fO_2 at which C and carbonate can coexist (Stagno *et al.* 2015). Although the effect of bulk-rock chemistry (Fig. 5a) mainly reflects on the composition of coexisting clinopyroxene and garnet used to calculate the fO_2 from equilibrium (11), carbonate minerals (or carbonatitic melts) are predicted to be stable down to the transition zone or lower mantle as a consequence of either the hot regime of the slab or its high ferric iron content inherited by the subducted altered oceanic crust or late-stage oxidizing processes. In both cases, diamonds in eclogites are expected to form at depths of 200–400 km, when the fO_2 buffered by the Fe-bearing silicate minerals crosses the appropriate carbon–carbonate equilibrium (dashed black line).

Ancient subduction in the early Earth was probably inefficient in transporting carbonates to depth owing to the predicted hot regime (Brown 2006), which would have caused decarbonation or melting at shallow conditions (*c.* 30–70 km; Dasgupta & Hirschmann 2010). Alternatively, the low potential of oxidation of the slab (low $Fe^{3+}/\Sigma Fe$) might have contributed to near-surface reduction of subducted carbonates to graphite (Fig. 5c), thus preventing CO_2 outgassing. Both scenarios would be in contrast to an origin of kimberlitic magmas during the Archean as in case of the Wawa kimberlites (Kopylova *et al.* 2011), therefore supporting their extreme rarity in the initial stage of Earth's history (Stern *et al.* 2016).

The mantle redox state and carbon extraction over time

The determination of the oxidation state of the asthenospheric mantle and subducting slab at depth has important implications for the mobilization and sequestration of carbon over time. Carbonate melts in the Earth's interior formed by oxidation of diamonds when the fO_2 buffered by the coexisting Fe-bearing silicates represented by the equilibria (10) and (11) intercepts the fO_2 at which carbon can coexist with carbonate as in equation (1) and (2). In Figure 4 the fO_2 for the stability of carbonate with respect to graphite or diamond in peridotitic rocks is calculated along a representative cratonic geotherm, and Figure 5 shows the fO_2 at which carbon and carbonate would coexist along a subducted slab taking into account important variables such as the different MORB chemical composition, *P*–*T* path and $Fe^{3+}/\Sigma Fe$ ratio of the protolith. The possibility for C-bearing rocks to melt is, therefore, dependent not only on the local thermal regimes but also, more importantly, on the temporal evolution of the mantle redox state that promotes oxidation of the refractory carbon to carbonate, promoting, therefore, redox melting processes (Stagno *et al.* 2013). Therefore, it is of fundamental importance to investigate the variation of the mantle redox state through time to better understand the mobilization of deep carbon through the history of the Earth.

Geochemical tracers such as the V/Sc ratio of erupted basalts have been widely used to claim the constancy of the mantle redox state over the last 3.8 Gyr (Li & Lee 2004; Scaillet & Gaillard 2011) to conditions where C is stable in the form of C^{4+}. Based on the reconstruction of the mantle oxidation state over time using the V/Sc of Archean eclogites as representative of early metabasalts, Aulbach & Stagno (2016) highlighted the possibility that the mantle underwent a gradual, rather than sudden, oxidation process during which the fO_2 was raised by *c.* 1 log unit to the modern MORB during the last 3.8 Gyr. Despite the large uncertainties in their fO_2 determinations, a similar conclusion was reached by Nicklas *et al.* (2018) through partitioning measurements of V in komatiites. Figure 6 is a schematic illustration that summarizes the redox melting of a diamond-bearing asthenospheric mantle from the Archean (Fig. 6a–d) to the present (Fig. 6e and f). The fO_2 of the mantle, which is indicated by straight lines calculated as a function of different $Fe^{3+}/\Sigma Fe$, is shown to increase toward shallower depths as a result of the decompression on the volume change of equation (10) until the carbon–carbonate equilibrium (i.e. equilibrium (1)) is crossed and carbonatitic melts form by redox melting. This probably happened during the early Archean (3 Ga) when, owing to the hot mantle adiabat and the low $Fe^{3+}/\Sigma Fe$ (assumed to be 2% for a reduced upper mantle), carbonate–silicate melts formed at about FMQ −2 log units at *c.* 100 km depth. Small amounts of carbonated silicate melts could be produced owing to the limited amount of carbon (*c.* 10 ppm in the case of reduced Early Earth; Dasgupta 2013), which, once entirely oxidized, led the Archean mantle redox state to further increase to the fO_2 indicated by the Archean MORB (FMQ −1.5 log units) represented by the Lace metabasaltic eclogite (Aulbach & Stagno 2016). Figure 6c and d shows that the thickness that undergoes redox melting strictly depends on the initial mantle $Fe^{3+}/\Sigma Fe$ ratio and carbon content according to equilibrium (12). The gradual increase of Fe^{3+} in the bulk asthenospheric mantle through time owing to subduction of oxidized material (Arculus 1985) resulted in the deepening of the redox melting with consequent decrease in the fraction of carbonatitic melts and their dilution during ascent (Fig. 6e and f). The composition of these magmas remains strictly controlled by the temperature and pressure, varying from carbonatitic to carbonate–silicate to basalts during upwelling with an increase in the melt fraction from less than 0.01 vol% to *c.* 10 vol%. It is expected, therefore, that the rheological properties of these melts such as viscosity and ascent rate will continuously change upon upwelling as they dilute to the more abundant MORB by about three orders of magnitude (Kono *et al.* 2014; Stagno *et al.* 2018). The drawn models have a two-fold implication: (1) that the oxidation state of MORB does not reflect the mantle oxidation state at the source, although it is linked to it (see Sorbadere *et al.* 2018, after reading Ballhaus 1993); (2) that larger volumes of CO_2-rich melts could have formed at shallower conditions during the Archean when the convective mantle was less oxidized and more 'hot', to then become less and less abundant to the present as a result of dilution at depth.

The carbon speciation in the transition zone and lower mantle

Previous experimental studies provided evidence of metal saturation at pressures compatible with the transition zone and the lower mantle, which implies that diamond is the most stable form of carbon in the Earth's deep interior (Frost *et al.* 2004; Rohrbach *et al.* 2011). The discovery of crystallized carbonated melts (Walter *et al.* 2008), calcite (Brenker *et al.* 2007), dolomite (Bulanova *et al.* 2010) and other carbonate minerals (Kaminsky 2012) all trapped in natural sub-lithospheric diamonds provided an alternative view of the deep mantle as characterized by higher oxygen fugacities where metal iron would not exist. Estimates of the fO_2 at which carbonate and diamond can coexist (e.g. the trapped carbonate inclusions in diamonds) can be determined through thermodynamic calculations (see equations (5)–(7)) using similar equilibria to equations (1) and (2) but employing the appropriate high-pressure polymorphs (wadsleyite or ringwoodite, coesite or stishovite, clinoenstatite, etc.). As an example, the equilibrium

$$\underset{\text{magnesite}}{MgCO_3} = \underset{\text{periclase}}{MgO} + \underset{\text{diamond}}{C} + O_2 \qquad (13)$$

is chosen to represent the coexistence of magnesite and diamond in the lower mantle along with periclase intended here as a component

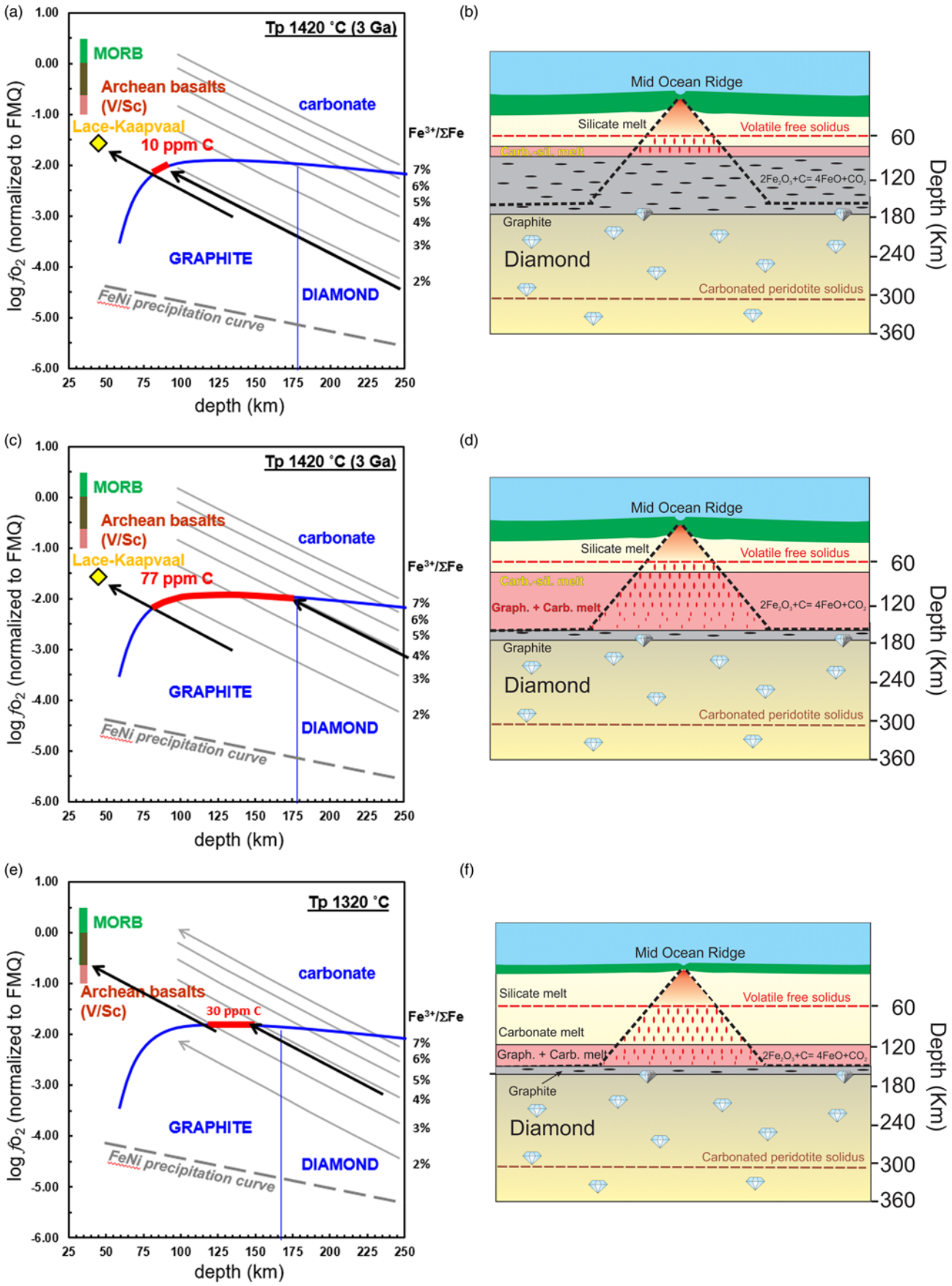

Fig. 6. (**a**–**f**) Thermodynamic prediction of the variation of the mantle oxidation state upon decompression obtained using equilibrium (10), and consequent depth at which the redox melting would occur. Detailed calculations have been given by Stagno *et al.* (2013) and Aulbach & Stagno (2016).

of ferropericlase. Unfortunately, thermodynamic calculations of the fO_2 can result in contrasting results owing to uncertain available data used to describe the compressibility of mineral end-members as a function of pressure and temperature (i.e. bulk modulus and its pressure derivative). This is the case shown in Figure 7, where two different log fO_2 versus pressure trends are obtained depending on

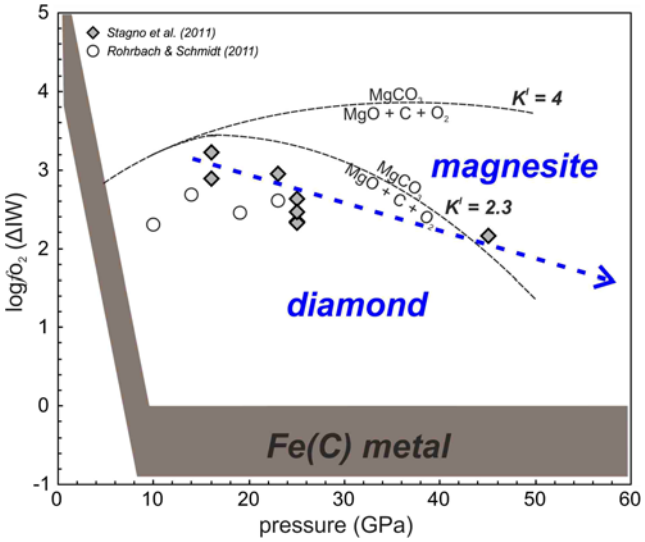

Fig. 7. Experimental measurements of the fO_2 (relative to IW) v. pressure for magnesite and diamond to coexist (blue dashed line), along with transition zone and lower mantle mineral phases obtained using the IrFe alloy redox sensor and compared with thermodynamic calculations through (equation (13)) changing EoS data for magnesite (Fiquet *et al.* 1994; Ross 1997; Litasov *et al.* 2008). The dark shaded region indicates the fO_2 of the mantle after Frost & McCammon (2008) and Stagno & Frost (2010) calculated along a mantle adiabat to 10 GPa.

the equation of state (EoS) data used for magnesite. For this reason, Stagno *et al.* (2011) determined experimentally the fO_2 at which diamond and magnesite can coexist in mineral assemblages consisting respectively of wadsleyite (or ringwoodite) plus clinoenstatite, and ferropericlase plus bridgmanite synthesized at pressures from 16 to *c.* 50 GPa using the redox sensor technique described above. These values were found to be about 2 log units above the iron–wüstite (IW) buffer, which implies that diamonds hosting carbonate inclusions are witnesses of more oxidized conditions in the deep interior than previously thought. From Figure 7, it can be noted that by extrapolating these measured values

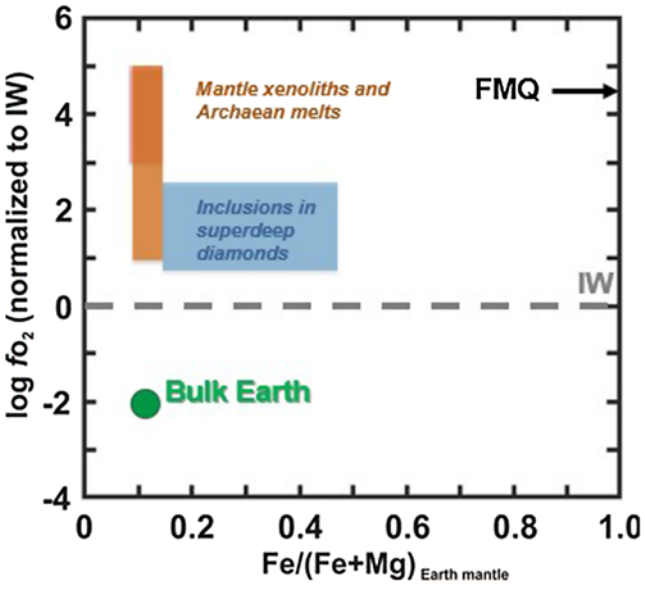

Fig. 8. Log fO_2 v. Fe# (Fe/(Fe + Mg)) of mantle rocks (orange rectangle) and ferropericlase inclusions in superdeep diamonds (blue area) along with that of the Earth at the core–mantle separation (green circle; Frost *et al.* 2008). The pink shaded area refers to fO_2 (between 3 and 5 log units to IW) of present-day MORB.

at high pressures of 100 GPa or so, magnesite is expected to be stable along with diamonds and Fe (maybe with some dissolved C), which is in agreement with the observed stability of magnesite (Isshiki *et al.* 2004) at lower mantle depths. More importantly, the presence of about 9000 ppm of C in the form of magnesite would be required to raise the fO_2 in the lower mantle by 2 log units relative to the IW buffer, causing, therefore, oxidation of 1% Fe metal (Rohrbach & Schmidt 2011) and incorporation of about 60% and about 2% of Fe^{3+}/Fe_{tot} in bridgmanite and ferropericlase, respectively (Stagno *et al.* 2011).

Whether carbonates (solid or liquid) can be stable in the transition zone or lower mantle in subducted MORB-like lithologies strictly links with the role of coexisting Fe-bearing redox-sensitive minerals such as majoritic garnet, tetragonal almandine–pyrope phase (TAPP), new hexagonal aluminous (NAL) phase, calcium-ferrite (CF) and bridgmanite phases. These phases are all possible candidates for incorporating large amounts of Fe^{3+} at transition zone and lower mantle conditions during subduction, leading to the formation of sub-lithospheric diamonds from the oxidized CO_2-bearing fluids. Potential equilibria such as equations (1) and (2) might be written that involve some of these phases plus carbonate and diamond. However, to date no experimental studies have been performed to determine the effect of fO_2, pressure and temperature on their Fe^{3+} content (i.e. their redox buffering capacity).

Conclusions

For decades, the experimental investigation of melting processes in the interior of the Earth has relied mostly on the effect of volatile elements in their oxidized state where C has been considered to be stable as CO_2 at any depth, playing, therefore, the major role in lowering the melting temperature of mantle rocks and causing the formation of carbonate magmas. However, the redox state of the Earth's interior has played a major role in controlling the oxidation and reduction of C species and its geodynamic cycle over time, and the evolution of the mantle redox state can be investigated through the application of oxy-thermobarometry on dated mantle rocks. Such studies, along with the mineralogical findings in (sub) lithospheric diamonds, have raised several important questions, such as: When does carbon turn into carbonate at mantle conditions? What is the minimum amount of oxygen required to oxidize elemental carbon to CO_2 within natural deep mineral assemblages? Has the increase of the mantle redox state been a gradual process or did it occur all at once? Is it possible to link the mantle redox state to the volcanic eruptive style and the migration rate of magmas from the mantle up to the surface? The seismic evidence of low-velocity zones is often referred to the presence of incipient melting processes, but this would imply stagnation of melt rather than fast ascent rate (Stagno *et al.* 2018). Are Fe-bearing minerals valid indicators of oxidized conditions and melting processes in the hidden deep mantle?

Recent studies have provided geochemical evidence of a gradual increase in fO_2 (Aulbach & Stagno 2016; Nicklas *et al.* 2018) in contrast to the general view that the mantle retained a constant fO_2 of IW +4(±1) (Scaillet & Gaillard 2011) over the last 4 Gyr (Trail *et al.* 2011). Figure 8 summarizes the redox state of the Earth's mantle from the fO_2 of abyssal peridotites (Frost & McCammon 2008), present-day and Archean MORB (Aulbach & Stagno 2016), and diamonds with (Mg,Fe)O inclusions that are variable in Fe# [Fe/(Fe + Mg)] for which the fO_2 is inferred by the presence of carbonate inclusions (Kaminsky 2012) through Figure 7. The fO_2 of Earth at the time of equilibration (separation) between mantle and core is also shown in Figure 7 (green circle; Frost *et al.* 2008). Interestingly, this figure indicates that the mantle redox state is distinct between the lower and the upper mantle, as well as heterogeneous in both C-reservoirs with fO_2 values ranging up to *c.* 5 log units relative to the IW buffer. This implies that the mobilization of carbon over time

does not necessarily require a mantle great oxidation event to occur (*c.* IW +1); in contrast, local chemical heterogeneities, pressure effect on the carbon–carbonate equilibria and kinetics of the redox reactions such as equation (12) might have played a key role over time.

Acknowledgements The critical and thoughtful comments by the two reviewers, S. Mikhail and T. Hammouda, are gratefully acknowledged and helped to improve the quality of this paper. Special thanks go to editors M. L. Frezzotti and I. Villa for their patience during the preparation of this paper. I would like to dedicate this manuscript to Professor Mariano Valenza, who suddenly passed away a few months before the final submission. Most of the motivation in my own research exists thanks to what I learnt from him throughout 2006. Much of what is discussed in this paper would not have been possible without the comprehension of my wife Paola Valenti over the last 12 years while travelling around the world to perform new exciting experiments with the support by colleagues at Bayerisches Geoinstitut (Bayreuth), Geophysical Laboratory (Carnegie Institution of Washington), and Geodynamics Research Center (Ehime University).

Funding V.S. acknowledges financial support by the DeepCarbon Observatory (DCO), Sloan funds (G2016-7282) and Sapienza University of Rome through 'Fondi di Ateneo'.

Scientific editing by Maria Luce Frezzotti

References

Akaishi, M., Kanda, H. & Yamaoka, S. 1990. Synthesis of diamond from graphite–carbonate system under very high temperature and pressure. *Journal of Crystal Growth*, **104**, 578–581, https://doi.org/10.1016/0022-0248(90)90159-I

Arculus, R.J. 1985. Oxidation status of the mantle: past and present. *Annual Review of Earth and Planetary Sciences*, **13**, 75–95, https://doi.org/10.1146/annurev.ea.13.050185.000451

Aulbach, S. & Stagno, V. 2016. Evidence for a reducing Archean ambient mantle and its effects on the carbon cycle. *Geology*, **44**, 751–754, https://doi.org/10.1130/G38070.1

Aulbach, S. & Viljoen, K.S. 2015. Eclogite xenoliths from the Lace kimberlite, Kaapvaal craton: from convecting mantle source to palaeo-ocean floor and back. *Earth and Planetary Science Letters*, **431**, 274–286, https://doi.org/10.1016/j.epsl.2015.08.039

Aulbach, S., Woodland, A.B., Vasilyev, P., Galvez, M.E. & Viljoen, K.S. 2017. Effects of low-pressure igneous processes and subduction on $Fe^{3+}/\Sigma Fe$ and redox state of mantle eclogites from Lace (Kaapvaal craton). *Earth and Planetary Science Letters*, **474**, 283–295, https://doi.org/10.1016/j.epsl.2017.06.030

Ballhaus, C. 1993. Redox states of lithospheric and asthenospheric upper mantle. *Contributions to Mineralogy and Petrology*, **114**, 331–348, https://doi.org/10.1007/BF01046536

Ballhaus, C., Berry, R.F. & Green, D.H. 1991. High pressure experimental calibration of the olivine–orthopyroxene–spinel oxygen geobarometer: implications for the oxidation state of the upper mantle. *Contributions to Mineralogy and Petrology*, **107**, 27–40, https://doi.org/10.1007/BF00311183

Barrenechea, J.F., Luque, F.J., Rodas, M. & Pasteris, J.D. 1997. Vein-type graphite mineralization in the Jurassic volcanic rocks of the external zone of the Betic Cordillera (southern Spain). *Canadian Mineralogist*, **35**, 1379–1390.

Biellmann, C., Gillet, P., Guyot, F., Peyronneau, J. & Reynard, B. 1993. Experimental evidence for carbonate stability in the Earth's lower mantle. *Earth and Planetary Science Letters*, **118**, 31–41, https://doi.org/10.1016/0012-821X(93)90157-5

Boulard, E., Menguy, N. *et al.* 2012. Experimental investigation of the stability of Fe-rich carbonates in the lower mantle. *Journal of Geophysical Research: Solid Earth*, **117**, B02208, https://doi.org/10.1029/2011JB008733

Boyd, F.R. & Gurney, J.J. 1986. Diamonds and the African lithosphere. *Science*, **232**, 472–477, https://doi.org/10.1126/science.232.4749.472

Brenker, F.E., Vollmer, C. *et al.* 2007. Carbonates from the lower part of transition zone or even the lower mantle. *Earth and Planetary Science Letters*, **260**, 1–9, https://doi.org/10.1016/j.epsl.2007.02.038

Brown, M. 2006. Duality of thermal regimes is the distinctive characteristic of plate tectonics since the Neoarchean. *Geology*, **34**, 961–964, https://doi.org/10.1130/G22853A.1

Bulanova, G.P., Walter, M.J., Smith, C.B., Kohn, S.C., Armstrong, L.S., Blundy, J. & Gobbo, L. 2010. Mineral inclusions in sublithospheric diamonds from Collier 4 kimberlite pipe, Juina, Brazil: subducted protoliths, carbonated melts and primary kimberlite magmatism. *Contributions to Mineralogy and Petrology*, **160**, 489–510, https://doi.org/10.1007/s00410-010-0490-6

Bundy, F.P. 1963. Direct conversion of graphite to diamond in static pressure apparatus. *Journal of Chemical Physics*, **38**, 631, https://doi.org/10.1063/1.1733716

Cemič, L. 2005. *Thermodynamics in Mineral Sciences: An Introduction*. Springer, Berlin.

Cerantola, V., Bykova, E. *et al.* 2017. Stability of iron-bearing carbonates in the deep Earth's interior. *Nature Communications*, **8**, 15960, https://doi.org/10.1038/ncomms15960

Cottrell, E. & Kelley, K.A. 2011. The oxidation state of Fe in MORB glasses and the oxygen fugacity of the upper mantle. *Earth and Planetary Science Letters*, **305**, 270, https://doi.org/10.1016/j.epsl.2011.03.014

Creighton, S., Stachel, T., Matveev, S., Höfer, H.E., McCammon, C. & Luth, R.W. 2009. Oxidation of the Kaapvaal lithospheric mantle driven by metasomatism. *Contributions to Mineralogy and Petrology*, **157**, 491–504, https://doi.org/10.1007/s00410-008-0348-3

Dasgupta, R. 2013. Ingassing, storage, and outgassing of terrestrial carbon through geologic time. *In*: Hazen, R.M., Jones, A.P. & Baross, J.A. (eds) *Carbon in Earth*. Mineralogical Society of America and Geochemical Society, Reviews in Mineralogy and Geochemistry, **75**, 183–229, https://doi.org/10.2138/rmg.2013.75.7.

Dasgupta, R. & Hirschmann, M.M. 2006. Melting in the Earth's deep upper mantle caused by carbon dioxide. *Nature*, **440**, 659–662, https://doi.org/10.1038/nature04612

Dasgupta, R. & Hirschmann, M.M. 2010. The deep carbon cycle and melting in Earth's interior. *Earth and Planetary Science Letters*, **298**, 1–13, https://doi.org/10.1016/j.epsl.2010.06.039

Dasgupta, R., Hirschmann, M.M. & Dellas, N. 2005. The effect of bulk composition on the solidus of carbonated eclogite from partial melting experiments at 3 GPa. *Contributions to Mineralogy and Petrology*, **149**, 288–305, https://doi.org/10.1007/s00410-004-0649-0

Day, H.W. 2012. A revised diamond–graphite transition curve. *American Mineralogist*, **97**, 52–62, https://doi.org/10.2138/am.2011.3763

Delano, J.W. 2001. Redox history of the Earth's interior since *c.* 3900 Ma: implications for prebiotic molecules. *Origins of Life and Evolution of the Biosphere*, **31**, 311–341, https://doi.org/10.1023/A:1011895600380

Dunn, R.A., Toomey, D.R., Detrick, R.S. & Wilcock, W.S.D. 2001. Continuous mantle melt supply beneath an overlapping spreading center on the East Pacific Rise. *Science*, **291**, 1955–1958, https://doi.org/10.1126/science.1057683

Eggler, D.H. & Baker, D.R. 1982. Reduced volatiles in the system C–O–H: implications to mantle melting, fluid formation, and diamond genesis. *High-Pressure Research in Geophysics*, 237–250, https://doi.org/10.1007/978-94-009-7867-6_19

Eugster, H.P. 1957. Heterogeneous reactions involving oxidation and reduction at high pressure and temperature. *Journal of Chemical Physics*, **26**, 1720.

Eugster, H.P. & Wones, D.R. 1962. Stability relations of the ferruginous biotite, annite. *Journal of Petrology*, **3**, 82–125, https://doi.org/10.1093/petrology/3.1.82

Evans, R.L., Tarits, P. *et al.* 1999. Asymmetric electrical structure in the mantle beneath the East Pacific Rise at 17°S. *Science*, **286**, 752–756, https://doi.org/10.1126/science.286.5440.752

Fabrchanaya, O., Saxena, S.K., Richet, P. & Westrum, E.F. (eds) 2004. *Thermodynamic Data, Models and Phase Diagrams in Multicomponent Oxide Systems*. Springer, Berlin.

Falloon, T.J. & Green, D.H. 1989. The solidus of carbonated, fertile peridotite. *Earth and Planetary Science Letters*, **94**, 364–370, https://doi.org/10.1016/0012-821X(89)90153-2

Falloon, T.J. & Green, D.H. 1990. Solidus of carbonated fertile peridotite under fluid-saturated conditions. *Geology*, **18**, 195–199, https://doi.org/10.1130/0091-7613(1990)018<0195:SOCFPU>2.3.CO;2

Fedortchouk, Y., Canil, D. & Carlson, J.A. 2005. Dissolution forms in Lac de Gras diamonds and their relationship to the temperature and redox state of kimberlite magma. *Contributions to Mineralogy and Petrology*, **150**, 54–69, https://doi.org/10.1007/s00410-005-0003-1

Fei, Y. 1995. Thermal expansion. *In*: Ahrens, T.J. (ed.) *Mineral Physics and Crystallography – a Handbook of Physical Constants*, 1st edn. American Geophysical Union, Washington, DC, 29–44.

Fei, Y. & Brosh, E. 2014. Experimental study and thermodynamic calculations of phase relations in the Fe–C system at high pressure. *Earth and Planetary Science Letters*, **408**, 155–162, https://doi.org/10.1016/j.epsl.2014.09.044

Field, S.W. & Haggerty, S.E. 1990. Graphitic xenoliths from the Jagersfontein kimberlite, South Africa: evidence for dominantly anhydrous melting and carbon deposition. *EOS Transactions, American Geophysical Union*, **71**, 658.

Fiquet, G., Guyot, F. & Itié, J.P. 1994. High-pressure X-ray diffraction study of carbonates – $MgCO_3$, $CaMg(CO_3)_2$, and $CaCO_3$. *American Mineralogist*, **79**, 15–23.

Frost, D.J. & McCammon, C.A. 2008. The redox state of the Earth's mantle. *Annual Review of Earth and Planetary Sciences*, **36**, 389–420, https://doi.org/10.1146/annurev.earth.36.031207.124322

Frost, D.J., Liebske, C., Langenhorst, F. & McCammon, C.A. 2004. Experimental evidence for the existence of iron-rich metal in the Earth's lower mantle. *Nature*, **428**, 409–412, https://doi.org/10.1038/nature02413

Frost, D.J., Mann, U., Asahara, Y. & Rubie, D.C. 2008. The redox state of the mantle during and just after core formation. *Philosophical Transactions of the Royal Society of London, Series A*, **366**, 4315–4337, https://doi.org/10.1098/rsta.2008.0147

Gaillard, F., Malki, M., Iacono-Marziano, G., Pichavant, M. & Scaillet, B. 2008. Carbonatite melts and electrical conductivity in the asthenosphere. *Science*, **322**, 1363–1365, https://doi.org/10.1126/science.1164446

Galvez, M., Beyssac, O., Martinez, I., Benzerara, K., Chaduteau, C., Malvoisin, B. & Malavieille, J. 2013. Graphite formation by carbonate reduction during subduction. *Nature Geoscience*, **6**, 473–477, https://doi.org/10.1038/ngeo1827

Ghosh, S., Ohtani, E., Litasov, K.D. & Terasaki, H. 2009. Solidus of carbonated peridotite from 10 to 20 GPa and origin of magnesiocarbonatites melt in the Earth's deep mantle. *Chemical Geology*, **262**, 17–28, https://doi.org/10.1016/j.chemgeo.2008.12.030

Goncharov, A.G. & Ionov, D.A. 2012. Redox state of deep offcraton lithospheric mantle: new data from garnet and spinel peridotites from Vitim, southern Siberia. *Contributions to Mineralogy and Petrology*, **164**, 731–745, https://doi.org/10.1007/s00410-012-0767-z

Gu, Y.J., Lerner-Lam, A.L., Dziewonski, A.M. & Ekstrom, G. 2005. Deep structure and seismic anisotropy beneath the East Pacific Rise. *Earth and Planetary Science Letters*, **232**, 259–272, https://doi.org/10.1016/j.epsl.2005.01.019

Gudfinnsson, G.H. & Presnall, D.C. 2005. Continuous gradations among primary kimberlitic, carbonatitic, melilitic, basaltic, picritic, and komatiitic melts in equilibrium with garnet lherzolite at 3–8 GPa. *Journal of Petrology*, **46**, 1645–1659, https://doi.org/10.1093/petrology/egi029

Gudmundsson, G. & Wood, B.J. 1995. Experimental tests of garnet peridotite oxygen barometry. *Contributions to Mineralogy and Petrology*, **119**, 56–67, https://doi.org/10.1007/BF00310717

Gurney, J.J. 1989. Diamonds. *In*: Ross, J., *et al.* (eds) *Kimberlites and Related Rocks*. Geological Society of Australia, Special Publications, **14**, 935–965.

Gurney, J.J., Hildebrand, P.R., Carlson, J.A., Fedortchouk, Y. & Dyck, D.R. 2004. The morphological characteristics of diamonds from the Ekati property, Northwest Territories, Canada. *Lithos*, **77**, 21–38, https://doi.org/10.1016/j.lithos.2004.04.033

Gurney, J.J., Helmstaedt, H.H., Richardson, S.H. & Shirey, S.B. 2010. Diamonds through time. *Economic Geology and the Bulletin of the Society of Economic Geologists*, **105**, 689–712, https://doi.org/10.2113/gsecongeo.105.3.689

Hammouda, T. 2003. High-pressure melting of carbonated eclogite and experimental constraints on carbon recycling and storage in the mantle. *Earth and Planetary Science Letters*, **214**, 357–368, https://doi.org/10.1016/S0012-821X(03)00361-3

Hammouda, T. & Keshav, S. 2015. Melting in the mantle in the presence of carbon: Review of experiments and discussion on the origin of carbonatites. *Chemical Geology*, **418**, 171–188, https://doi.org/10.1016/j.chemgeo.2015.05.018

Hauri, E.H., Shimuzu, N., Dieu, J.J. & Hart, S.R. 1993. Evidence for hotspot-related carbonatite metasomatism in the oceanic upper mantle. *Nature*, **365**, 221–227, https://doi.org/10.1038/365221a0

Hayden, L.A. & Watson, E.B. 2008. Grain boundary mobility of carbon in Earth's mantle: A possible carbon flux from the core. *Proceedings of the National Academy of Sciences of the USA*, **105**, 8537–8541, https://doi.org/10.1073/pnas.0710806105

Huebner, J.S. 1971. Buffering techniques for hydrostatic systems at elevated pressures. *In*: Ulmer, G.C. (ed.) *Research Techniques for High Pressure and High Temperature*. Springer, Berlin.

Ionov, D.A., Dupuy, C., O'Reilly, S.Y., Kopylova, M.G. & Genshaft, Y.S. 1993. Carbonated peridotite xenoliths from Spitsbergen: implications for trace element signature of mantle carbonate metasomatism. *Earth and Planetary Science Letters*, **119**, 283–297, https://doi.org/10.1016/0012-821X(93)90139-Z

Ionov, D.A., Ashchepkov, I. & Jagoutz, E. 2005. The provenance of fertile off-craton lithospheric mantle: Sr–Nd isotope and chemical composition of garnet and spinel peridotite xenoliths from Vitim, Siberia. *Chemical Geology*, **217**, 41–75, https://doi.org/10.1016/j.chemgeo.2004.12.001

Irifune, T., Kurio, A., Sakamoto, S., Inoue, T., Sumiya, H. & Funakoshi, K.I. 2004. Formation of pure polycrystalline diamond by direct conversion of graphite at high pressure and high temperature. *Physics of the Earth and Planetary Interiors*, **143–144**, 593–600, https://doi.org/10.1016/j.pepi.2003.06.004

Isshiki, M., Irifune, T. *et al.* 2004. Stability of magnesite and its high-pressure form in the lowermost mantle. *Nature*, **427**, 60–63, https://doi.org/10.1038/nature02181

Jacob, D.E. 2004. Nature and origin of eclogite xenoliths from kimberlites. *Lithos*, **77**, 295–316, https://doi.org/10.1016/j.lithos.2004.03.038

Javoy, M., Pineau, F. & Allègre, C.J. 1982. Carbon geodynamic cycle. *Nature*, **300**, 171–173, https://doi.org/10.1038/300171a0

Kaminsky, F.V. 2012. Mineralogy of the lower mantle: A review of 'super-deep' mineral inclusions in diamond. *Earth-Science Reviews*, **110**, 127–147, https://doi.org/10.1016/j.earscirev.2011.10.005

Kaminsky, F.V. & Wirth, R. 2011. Iron carbide inclusions in lower-mantle diamond from Juina, Brazil. *Canadian Mineralogist*, **49**, 555–572, https://doi.org/10.3749/canmin.49.2.555

Kasting, J.F., Eggler, D.H. & Raeburn, S.P. 1993. Mantle redox evolution and the oxidation state of the Archean atmosphere. *Journal of Geology*, **101**, 245–257, https://doi.org/10.1086/648219

Kelemen, P.B. & Manning, C.E. 2015. Reevaluating carbon fluxes in subduction zones, what goes down, mostly comes up. *Proceedings of the National Academy of Sciences of the USA*, **112**, E3997–E4006, https://doi.org/10.1073/pnas.1507889112

Kennedy, C.S. & Kennedy, G.C. 1976. The equilibrium boundary between graphite and diamond. *Journal of Geophysical Research*, **81**, 2467, https://doi.org/10.1029/JB081i014p02467

Keppler, H., Wiedenbeck, M. & Shcheka, S.S. 2003. Carbon solubility in olivine and the mode of carbon storage in the Earth's mantle. *Nature*, **424**, 414–416, https://doi.org/10.1038/nature01828

Keshav, S. & Gudfinnsson, G.H. 2010. Experimentally dictated stability of carbonated oceanic crust to moderately great depths in the Earth: Results from the solidus determination in the system CaO–MgO–Al_2O_3–SiO_2–CO_2. *Journal of Geophysical Research*, **115**, B05205, https://doi.org/10.1029/2009JB006457

Kessel, R., Beckett, J.R. & Stolper, E.M. 2003. Thermodynamic properties of the Pt–Fe system. *American Mineralogist*, **86**, 1003–1014, https://doi.org/10.2138/am-2001-8-907

Kiseeva, E.S., Litasov, K.D., Yaxley, G.M., Ohtani, E. & Kamenetsky, V.S. 2013. Melting and phase relations of carbonated eclogite at 9–21 GPa and the petrogenesis of alkali-rich melts in the deep mantle. *Journal of Petrology*, **54**, 1555–1583, https://doi.org/10.1093/petrology/egt023

Kono, Y., Kenney-Benson, C. *et al.* 2014. Ultralow viscosity of carbonate melts at high pressures. *Nature Communications*, **5**, 5091, https://doi.org/10.1038/ncomms6091

Kopylova, M.G., Afanasiev, V.P., Bruce, L.F., Thurston, P.C. & Ryder, J. 2011. Metaconglomerate preserves evidence for kimberlite, diamondiferous root and medium grade terrane of a pre-2.7 Ga Southern Superior protocraton. *Earth and Planetary Science Letters*, **312**, 213–225, https://doi.org/10.1016/j.epsl.2011.09.057

Kornprobst, J., Pineau, F., Degiovanni, R. & Dautria, J.M. 1987. Primary igneous graphite in ultramafic xenoliths: I. Petrology of the cumulate suite in alkali basalt near Tissemt (Egg éré, Algerian Sahara). *Journal of Petrology*, **28**, 293–311, https://doi.org/10.1093/petrology/28.2.293

Korsakov, A.V., Perraki, M., Zedgenizov, D.A., Bindi, L., Vandenabeele, P., Suzuki, A. & Kagi, H. 2010. Diamond–graphite relationships in ultrahigh-pressure metamorphic rocks from the Kokchetav Massif, Northern Kazakhstan. *Journal of Petrology*, **51**, 763–783, https://doi.org/10.1093/petrology/egq001

Koster van Groos, A.F. & Wyllie, P.J. 1963. Experimental data bearing on the role of liquid immiscibility in the genesis of carbonatites. *Nature*, **199**, 801–802, https://doi.org/10.1038/199801a0

Leung, I., Guo, W., Friedman, I. & Gleason, J. 1990. Natural occurrence of silicon carbide in a diamondiferous kimberlite from Fuxian. *Nature*, **346**, 352–354, https://doi.org/10.1038/346352a0

Le Voyer, M., Kelley, K., Cottrell, E. & Hauri, E. 2017. Heterogeneity in mantle carbon content from CO_2-undersaturated basalts. *Nature Communications*, **8**, 14062, https://doi.org/10.1038/ncomms14062

Li, Z.-X.A. & Lee, C.-T.A. 2004. The constancy of upper mantle fO_2 through time inferred from V/Sc ratios in basalts. *Earth and Planetary Science Letters*, **228**, 483–493, https://doi.org/10.1016/j.epsl.2004.10.006

Litasov, K.D. & Ohtani, E. 2009*a*. Phase relations in the peridotite–carbonate–chloride system at 7.0–16.5 GPa and the role of chlorides in the origin of kimberlite and diamond. *Chemical Geology*, **262**, 29–41, https://doi.org/10.1016/j.chemgeo.2008.12.027

Litasov, K. & Ohtani, E. 2009*b*. Solidus and phase relations of carbonated peridotite in the system CaO–Al_2O_3–MgO–SiO_2–Na_2O–CO_2 to the lower mantle depths. *Physics of the Earth and Planetary Interiors*, **177**, 46–58, https://doi.org/10.1016/j.pepi.2009.07.008

Litasov, K. & Ohtani, E. 2010. The solidus of carbonated eclogite in the system CaO–Al_2O_3–MgO–SiO_2–Na_2O–CO_2 to 32 GPa and carbonatite liquid in the deep mantle. *Earth and Planetary Science Letters*, **295**, 115–126, https://doi.org/10.1016/j.epsl.2010.03.030

Litasov, K.D., Fei, Y., Ohtani, E., Kuribayashi, T. & Funakoshi, K. 2008. Thermal equation of state of magnesite to 32 GPa and 2073 K. *Physics of the Earth and Planetary Interiors*, **168**, 191–203, https://doi.org/10.1016/j.pepi.2008.06.018

Liu, Y., He, D. *et al.* 2016. First direct evidence of sedimentary carbonate recycling in subduction-related xenoliths. *Scientific Reports*, **5**, 11547, https://doi.org/10.1038/srep11547

Llovet, X. & Galan, G. 2003. Correction of secondary X-ray fluorescence near grain boundaries in electron microprobe analysis: application to thermobarometry of spinel lherzolites. *American Mineralogist*, **88**, 121–130, https://doi.org/10.2138/am-2003-0115

Luque, F.J., Pasteris, J.D., Wopenka, B., Rodas, M. & Barrenechea, J.F. 1998. Natural fluid-deposited graphite: mineralogical characteristics and mechanisms of formation. *American Journal of Science*, **298**, 471–498, https://doi.org/10.2475/ajs.298.6.471

Lustrino, M., Prelevic, D., Agostini, S., Gaeta, M., Di Rocco, T., Stagno, V. & Capizzi, L.S. 2016. Ca-rich carbonates associated with ultrabasic–ultramafic melts: carbonatite or limestone xenoliths? A case study from the late Miocene Morron de Villamayor volcano (Calatrava volcanic field, central Spain). *Geochimica et Cosmochimica Acta*, **185**, 477–497, https://doi.org/10.1016/j.gca.2016.02.026

Luth, R.W. 1993. Diamonds, eclogites and the oxidation state of the Earth's mantle. *Science, New Series*, **261**, 66–68, https://doi.org/10.1126/science.261.5117.66

Mao, Z., Armentrout, M., Rainey, E., Manning, C.E., Dera, P., Prakapenka, V.B. & Kavner, A. 2011. Dolomite III: A new candidate lower mantle carbonate. *Geophysical Research Letters* **38**, L22303, https://doi.org/10.1029/2011GL049519

Marty, B., Alexander, C.M.O. & Raymond, S. 2013. Primordial origins of Earth's carbon. *In*: Hazen, R.M., Jones, A.P. & Baross, J.A. (eds) *Carbon in Earth*. Mineralogical Society of America and Geochemical Society, Reviews in Mineralogy and Geochemistry, **75**, 149–181, https://doi.org/10.2138/rmg.2013.75.6

Mathez, E.A., Fogel, R.A., Hutcheon, I.D. & Marshintsev, V.K. 1995. Carbon isotopic composition and origin of SiC from kimberlites of Yakutia, Russia. *Geochimica et Cosmochimica Acta*, **59**, 781–791, https://doi.org/10.1016/0016-7037(95)00002-H

Matthews, S., Shorttle, O., Rudge, J.F. & Maclennan, J. 2017. Constraining mantle carbon: CO_2–trace element systematics in basalts and the roles of magma mixing and degassing. *Earth and Planetary Science Letters*, **480**, 1–14, https://doi.org/10.1016/j.epsl.2017.09.047

McCammon, C.A. & Ross, N.L. 2003. Crystal chemistry of ferric iron in (Mg,Fe)(Si,Al)O_3 majorite with implications for the transition zone. *Physics and Chemistry of Minerals*, **30**, 206–216, https://doi.org/10.1007/s00269-003-0309-3

Meyer, H.O.A. 1987. Inclusions in diamonds. *In*: Nixon, P.H. (ed.) *Mantle Xenoliths*. Wiley, Chichester, 501–522.

Mikhail, S., Guillermier, C. *et al.* 2014. Empirical evidence for the fractionation of carbon isotopes between diamond and iron carbide from the Earth's mantle. *Geochemistry, Geophysics, Geosystems*, **15**, 855–866, https://doi.org/10.1002/2013GC005138

Mikhailenko, D.S., Korsakov, A.V., Zelenovskiy, P.S. & Golovin, A.V. 2016. Graphite–diamond relations in mantle rocks: Evidence from an eclogitic xenolith from the Udachnaya kimberlite (Siberian Craton). *American Mineralogist*, **101**, 2155–2167, https://doi.org/10.2138/am-2016-5657

Miller, W.G.R., Holland, T.J.B. & Gibson, S.A. 2016. Garnet and spinel oxybarometers: new internally consistent multi-equilibria models with applications to the oxidation state of the lithospheric mantle. *Journal of Petrology*, **57**, 1199–1222, https://doi.org/10.1093/petrology/egw037

Nicklas, R.W., Puchtel, I.S. & Ash, R.D. 2018. Redox state of the Archean mantle: Evidence from V partitioning in 3.5–2.4 Ga komatiites. *Geochimica et Cosmochimica Acta*, **222**, 447–466, https://doi.org/10.1016/j.gca.2017.11.002

Oganov, A.R., Ono, S., Ma, Y., Glass, C.W. & Garcia, A. 2008. Novel high-pressure structures of $MgCO_3$, $CaCO_3$ and CO_2 and their role in Earth's lower mantle. *Earth and Planetary Science Letters*, **273**, 38–47, https://doi.org/10.1016/j.epsl.2008.06.005

O'Neill, H.S.C. 1987. Quartz–fayalite–iron and quartz–fayalite–magnetite equilibria and the free energies of formation of fayalite (Fe_2SiO_4) and magnetite (Fe_3O_4). *American Mineralogist*, **72**, 67–75.

Palot, M., Cartigny, P., Harris, J.W., Kaminsky, F.V. & Stachel, T. 2012. Evidence for deep mantle convection and primordial heterogeneity from nitrogen and carbon stable isotopes in diamond. *Earth and Planetary Science Letters*, **357–358**, 179–193, https://doi.org/10.1016/j.epsl.2012.09.015

Palyanov, Y.N., Bataleva, Y.V., Sokol, A.G., Borzdov, Y.M., Kupriyanov, I.N., Reutsky, V.N. & Sobolev, N.V. 2013. Mantle–slab interaction and redox mechanism of diamond formation. *Proceedings of the National Academy of Sciences of the USA*, **110**, 20408–20413, https://doi.org/10.1073/pnas.1313340110

Pearson, D.G., Davies, G.R., Nixon, P.H. & Milledge, H.J. 1989. Graphitized diamonds from a peridotite massif in Morocco and implications for anomalous diamond occurrences. *Nature*, **338**, 60–62, https://doi.org/10.1038/338060a0

Ripley, E.M. & Taib, N.I. 1989. Carbon isotopic studies of metasedimentary and igneous rocks at the Babbitt Cu–Ni deposit, Duluth Complex, Minnesota, U.S.A. *Chemical Geology*, **73**, 319–342, https://doi.org/10.1016/0168-9622(89)90025-0

Rohrbach, A. & Schmidt, M.W. 2011. Redox freezing and melting in the Earth's deep mantle resulting from carbon–iron redox coupling. *Nature*, **472**, 209–212, https://doi.org/10.1038/nature09899

Rohrbach, A., Ballhaus, C., Ulmer, P., Golla-Schindler, U. & Schönbohm, D. 2011. Experimental evidence for a reduced metal-saturated upper mantle. *Journal of Petrology*, **52**, 717–731, https://doi.org/10.1093/petrology/egq101

Rohrbach, A., Ghosh, S., Schmidt, M.W., Wijbrans, C.H. & Klemme, S. 2014. The stability of Fe–Ni carbides in the Earth's mantle: Evidence for a low Fe–Ni–C melt fraction in the deep mantle. *Earth and Planetary Science Letters*, **388**, 211, https://doi.org/10.1016/j.epsl.2013.12.007

Rosenthal, A., Yaxley, G.M., Green, D.H., Hermann, J., Kovács, I. & Spandler, C. 2014. Continuous eclogite melting and variable refertilisation in upwelling heterogeneous mantle. *Scientific Reports*, **4**, 6099, https://doi.org/10.1038/srep06099

Rosenthal, A., Hauri, E. & Hirschmann, M. 2015. Experimental determination of C, F, and H partitioning between mantle minerals and carbonated basalt, CO_2/Ba and CO_2/Nb systematics of partial melting, and the CO_2 contents of basaltic source regions. *Earth and Planetary Science Letters*, **412**, 77–87, https://doi.org/10.1016/j.epsl.2014.11.044

Ross, N.L. 1997. The equation of state and high-pressure behavior of magnesite. *American Mineralogist*, **82**, 682–688, https://doi.org/10.2138/am-1997-7-805

Rubie, D.C. 1999. Characterising the sample environment in multi anvil high-pressure experiments. *Phase Transitions*, **68**, 431–451, https://doi.org/10.1080/01411599908224526

Scaillet, B. & Gaillard, F. 2011. Redox state of early magmas. *Nature*, **480**, 48–49, https://doi.org/10.1038/480048a

Schmidt, M.W., Gao, C., Golubkova, A., Rohrbach, A. & Connolly, J.A.D. 2014. Natural moissanite (SiC) – a low temperature mineral formed from highly fractionated ultra-reducing COH-fluids. *Progress in Earth and Planetary Science*, **1**, 27, https://doi.org/10.1186/s40645-014-0027-0

Schwerdtfeger, K. & Zwell, U. 1968. Activities in solid iridium–iron and rhodium–iron alloys at 1200°C. *Transactions of the Metallurgical Society of AIME*, **242**, 631–633.

Shatskiy, A., Litasov, K.D., Ohtani, E., Borzdov, Y.M., Khmelnikov, A.I. & Palyanov, Y.N. 2015*a*. Phase relations in the K_2CO_3–$FeCO_3$ and $MgCO_3$–$FeCO_3$ systems at 6 GPa and 900–1700°C. *European Journal of Mineralogy*, **27**, 487–499, https://doi.org/10.1127/ejm/2015/0027-2452

Shatskiy, A., Rashchenko, S.V. *et al.* 2015*b*. The system Na_2CO_3–$FeCO_3$ at 6 GPa and its relation to the system Na_2CO_3–$FeCO_3$–$MgCO_3$. *American Mineralogist*, **100**, 130–137, https://doi.org/10.2138/am-2015-4777

Shcheka, S.S., Weidenbeck, M., Frost, D.J. & Keppler, H. 2006. Carbon solubility in mantle minerals. *Earth and Planetary Science Letters*, **245**, 730–742, https://doi.org/10.1016/j.epsl.2006.03.036

Smith, E.M., Shirey, S., Nestola, F., Bullock, E.S., Wang, J., Richardson, S. & Wang, W. 2016. Large gem diamonds from metallic liquid in Earth's deep mantle. *Science*, **354**, 1403–1405, https://doi.org/10.1126/science.aal1303

Smyth, J.R. 1980. Cation vacancies and the crystal chemistry of breakdown reactions in kimberlitic omphacites. *American Mineralogist*, **65**, 1257–1264.

Solopova, N., Dubrovinsky, L., Spivak, A., Litvin, Y. & Dubrovinskaia, N. 2014. Melting and decomposition of $MgCO_3$ at pressures up to 84 GPa. *Physics and Chemistry of Minerals*, **42**, https://doi.org/10.1007/s00269-014-0701-1

Sorbadere, F., Laurenz, V., Frost, D.J., Wenz, M., Rosenthal, A., McCammon, C. & Rivard, C. 2018. The behaviour of ferric iron during partial melting of peridotite. *Geochimica et Cosmochimica Acta*, **239**, 235–254, https://doi.org/10.1016/j.gca.2018.07.019

Stachel, T. & Harris, J.W. 2008. The origin of cratonic diamond – constraints from mineral inclusions. *Ore Geology Reviews*, **34**, 5–32, https://doi.org/10.1016/j.oregeorev.2007.05.002

Stagno, V. & Frost, D.J. 2010. Carbon speciation in the asthenosphere: Experimental measurements of the redox conditions at which carbonate-bearing melts coexist with graphite or diamond in peridotite assemblages. *Earth and Planetary Science Letters*, **300**, 72–84, https://doi.org/10.1016/j.epsl.2010.09.038

Stagno, V., Tange, Y., Miyajima, N., McCammon, C.A., Irifune, T. & Frost, D.J. 2011. The stability of magnesite in the transition zone and the lower mantle as function of oxygen fugacity. *Geophysical Research Letters*, **38**, L19309, https://doi.org/10.1029/2011GL049560

Stagno, V., Ojwang, D.O., McCammon, C.A. & Frost, D.J. 2013. The oxidation state of the mantle and the extraction of carbon from Earth's interior. *Nature*, **493**, 84–88, https://doi.org/10.1038/nature11679

Stagno, V., Crispin, K. L., Shahar, A. & Fei, Y. 2014. Growth kinetics of a reaction rim between iron and graphite/diamond and the carbon diffusion mechanism at high pressure and temperature. *AGU Fall Meeting Abstracts*, V13A-4743.

Stagno, V., Frost, D.J., McCammon, C.A., Mohseni, H. & Fei, Y. 2015. The oxygen fugacity at which graphite or diamond forms from carbonate-bearing melts in eclogitic rocks. *Contributions to Mineralogy and Petrology*, **169**, 16, https://doi.org/10.1007/s00410-015-1111-1

Stagno, V., Stopponi, V., Kono, Y., Manning, C.E. & Irifune, T. 2018. Experimental determination of the viscosity of Na_2CO_3 melt between 1.7 and 4.6 GPa at 1200–1700°C: Implications for the rheology of carbonatite magmas in the Earth's upper mantle. *Chemical Geology*, **501**, 19–25, https://doi.org/10.1016/j.chemgeo.2018.09.036

Stern, R.J., Leybourne, M.I. & Tsujimori, T. 2016. Kimberlites and the start of plate tectonics. *Geology*, **44**, 799–802, https://doi.org/10.1130/G38024.1

Streckeisen, A. 1980. Classification and nomenclature of volcanic rocks, lamprophyres, carbonatites and melilitic rocks. IUGS Subcommission on the Systematics of Igneous Rocks. *Geologische Rundschau*, **69**, 194–207, https://doi.org/10.1007/BF01869032

Syracuse, E.M., van Keken, P.E. & Abers, G.A. 2010. The global range of subduction zone thermal models. *Physics of the Earth and Planetary Interiors*, **183**, 73–90, https://doi.org/10.1016/j.pepi.2010.02.004

Tao, R.B., Fei, Y. & Zhang, L.F. 2013. Experimental determination of siderite stability at high pressure. *American Mineralogist*, **98**, 1565–1572, https://doi.org/10.2138/am.2013.4351

Taylor, J., Wall, V.J. & Pownceby, M.I. 1992. The calibration and application of accurate redox sensors. *American Mineralogist*, **77**, 284–295.

Thomson, A.R., Walter, M.J., Kohn, S.C. & Brooker, R.A. 2016. Slab melting as a barrier to deep carbon subduction. *Nature*, **529**, 76–79, https://doi.org/10.1038/nature16174

Trail, D., Watson, E.B. & Tailby, N.D. 2011. The oxidation state of Hadean magmas and implications for early Earth's atmosphere. *Nature*, **480**, 79–82, https://doi.org/10.1038/nature10655

Ulmer, P. & Luth, R.W. 1991. The graphite–COH fluid equilibrium in P, T, fO_2 space. *Contributions to Mineralogy and Petrology*, **106**, 265–272, https://doi.org/10.1007/BF00324556

Ulmer, G., Grandstaff, D.E., Woermann, E., Göbbels, M., Schönitz, M. & Woodland, A.B. 1997. The redox stability of moissanite (SiC) compared with metal–metal oxide buffers at 1773 K and at pressures up to 90 kbar. *Neues Jahrbuch für Mineralogie, Abhandlungen*, **172**, 279–307.

Veksler, I.V., Nielsen, T.F.D. & Sokolov, S.V. 1998. Mineralogy of crystallized melt inclusions from Gardiner and Kovdor ultramafic alkaline complexes: implications for carbonatite petrogenesis. *Journal of Petrology*, **39**, 2015–2031, https://doi.org/10.1093/petroj/39.11-12.2015

Wallace, M.E. & Green, D.H. 1988. An experimental determination of primary carbonatite magma composition. *Nature*, **335**, 343–346, https://doi.org/10.1038/335343a0

Walter, M., Bulanova, G. *et al.* 2008. Primary carbonatite melt from deeply subducted oceanic crust. *Nature*, **454**, 622–625, https://doi.org/10.1038/nature07132

Weiss, Y., Griffin, W.L., Bell, D.R. & Navon, O. 2011. High-Mg carbonatitic melts in diamonds, kimberlites and the sub-continental lithosphere. *Earth and Planetary Science Letters*, **309**, 337–347, https://doi.org/10.1016/j.epsl.2011.07.012

Wendlandt, R.F., Huebner, J.S. & Harrison, W.J. 1982. The redox potential of boron nitride and implications for its use as a crucible material in experimental petrology. *American Mineralogist*, **67**, 170–174.

Woolley, A.R. & Kempe, D.R.C. 1989. Carbonatites: Nomenclature, average chemical compositions and element distribution. *In*: Bell, K. (ed.) *Carbonatites: Genesis and Evolution*. Unwin Hyman, London, 1–14.

Woolley, A.R. & Kjarsgaard, B.A. 2008. *Carbonatite Occurrences of the World: Map and Database*. Geological Survey of Canada, Open File, **5796**.

Wyllie, P.J. & Huang, W.L. 1975. Influence of mantle CO_2 in the generation of carbonatites and kimberlites. *Nature*, **257**, 297–299, https://doi.org/10.1038/257297a0

Yang, J., Meng, F. *et al.* 2015. Diamonds, native elements and metal alloys from chromitites of the Ray-Iz ophiolite of the Polar Urals. *Gondwana Research*, **27**, 459–485, https://doi.org/10.1016/j.gr.2014.07.004

Yaxley, G.M. & Brey, G.P. 2004. Phase relations of carbonate-bearing eclogite assemblages from 2.5 to 5.5 GPa: implications for petrogenesis of carbonatites. *Contributions to Mineralogy and Petrology*, **146**, 606–619, https://doi.org/10.1007/s00410-003-0517-3

Yaxley, G.M. & Green, D.H. 1994. Experimental demonstration of refractory carbonate-bearing eclogite and siliceous melt in the subduction regime. *Earth and Planetary Science Letters*, **128**, 313–325, https://doi.org/10.1016/0012-821X(94)90153-8